QC
879.25
B422
v.2

7304050 3

FR-1110-104

APPENDIX TO FINAL REPORT

TIROS OPERATIONAL VERTICAL SOUNDER - BASIC SOUNDER UNIT

Subtask: Optics Design and Test Report

By B. D. Henderson

Purchase Order No. 01884

February 9, 1973

Prepared for:

Gulton Industries, Inc.
Data Systems Division
Albuquerque, N. M.

Beckman® INSTRUMENTS, INC.
ADVANCED TECHNOLOGY OPERATIONS
ANAHEIM, CALIFORNIA 92806

A
QC
879.25
B422
v.2

APPENDIX TO FINAL REPORT

TIROS OPERATIONAL VERTICAL SOUNDER - BASIC SOUNDER UNIT

Subtask: Optics Design and Test Report

By B. D. Henderson

Purchase Order No. 01884

February 9, 1973

ATMOSPHERIC SCIENCES
LIBRARY
MAY 1973
N.O.A.A.
U. S. Dept. of Commerce

Prepared for:

Gulton Industries, Inc.
Data Systems Division
Albuquerque, N. M.

Beckman® INSTRUMENTS, INC.
ADVANCED TECHNOLOGY OPERATIONS
ANAHEIM, CALIFORNIA 92806

15 .S64

National Oceanic and Atmospheric Administration
TIROS Satellites and Satellite Meteorology

ERRATA NOTICE

One or more conditions of the original document may affect the quality of the image, such as:

Discolored pages
Faded or light ink
Binding intrudes into the text

This has been a co-operative project between the NOAA Central Library and the Climate Database Modernization Program, National Climate Data Center (NCDC). To view the original document contact the NOAA Central Library in Silver Spring, MD at (301) 713-2607 x124 or Library.Reference@noaa.gov.

HOV Services
Imaging Contractor
12200 Kiln Court
Beltsville, MD 20704-1387
January 26, 2009

Beckman® INSTRUMENTS, INC.
ADVANCED TECHNOLOGY OPERATIONS
2500 HARBOR BOULEVARD, FULLERTON, CALIFORNIA • 92634
(714) 871-4848; TWX: 714-871-1790 • TELEX: 06-70813

Document No. FR 1110-104--APPENDIX
Rev_____ Rev Date_____

TITLE: TIROS OPERATIONAL VERTICAL SOUNDER - BASIC SOUNDER UNIT
Subtask: Optics Design and Test Report

Prepared For: Gulton Industries, Inc.
Data Systems Division
Albuquerque, N. M.

Prepared by: B. Henderson (Originator)	2-9-73 (Date)	Approved by: J. Morgan	2-9-73 (Date)
Approved by: (Project Engineer)	(Date)	Approved by:	(Date)
Approved by: T. O. Maley (Program Manager)	2/9/72 (Date)	Approved by:	(Date)
Approved by: B. D. Brown (Data Manager)	2/9/72 (Date)	Approved by:	(Date)

CONTENTS

PARAGRAPH		PAGE
1.0	INTRODUCTION	1-1
2.0	RAY-TRACE DESCRIPTION	2-1
3.0	TELESCOPE DESIGN	3-1
3.1	Telescope Requirements	3-1
3.2	Choice of Telescope Type	3-1
3.3	A Comparative Analysis of a Double-Sphere Cassegrainian Telescope and a Paraboloid-Hyperboloid Cassegrainian Telescope	3-2
3.4	Dimensional Parameters for the 80- and 61-mm OD TOVS-BSU Telescopes	3-3
3.5	Angular Field-of-View Image Characteristics for the 61- and 80-mm OD Telescope	3-3
3.6	Light Shield for a Cassegrainian Telescope	3-12
3.7	Dimple in Center of Telescope Secondary Mirror	3-14
3.8	Error Analysis for the Double-Sphere Telescopes	3-14
4.0	DETECTOR OPTICAL SYSTEM	4-1
4.1	Optical Arrangement and Function of Detector Optics	4-1
4.2	Design of Detector Optics for Each of the Fourteen Channels	4-1
4.3	Design and Performance of the Detector Doublet Lenses	4-28
4.4	Error Analysis for the Detector Optical System	4-54
5.0	DESIGN OF CHOPPER AND REFERENCE BLACKBODY	5-1

LIST OF TABLES

TABLE NO.		PAGE
2-1	Definitions for Ray-Trace Dimensional Parameters (2 Sheets)	2-2
2-2	Definitions for the Resultant Ray-Surface Intercepts and the Terminology for the Resultant Lateral Image Characteristics (2 Sheets)	2-4
2-3	Definitions for the Resultant Ray Direction Cosines and the Terminology for the Resultant Angular Image Characteristics (2 Sheets)	2-6
3-1	Comparative Angular Field-of-View Characteristics for the ITPR Double-Sphere Cassegrainian Telescope, and a Paraboloid-Hyperboloid Cassegrainian Telescope of the Same Size	3-4
3-2	Description of the Ray-Trace Axis Systems for both the 80- and 61-mm OD Double-Sphere Cassegrainian Telescopes	3-6
3-3	Dimensional Parameters for 80-mm OD Telescope	3-7
3-4	Dimensional Parameters for 61-mm OD Telescope	3-8
3-5	Angular Field-of-View Characteristics for the 80- and 61-mm OD Double-Sphere Cassegrainian Telescopes	3-10
3-6	TOVS-BSU and ITPR Double-Sphere Telescope Specifications	3-13
3-7	Dimensional Parameters for 61-mm OD Telescope Error Analysis	3-17
3-8	Error Analysis for 61-mm Telescope	3-18
3-9	Dimensional Tolerances for One-Percent Field Stop Error for 61-mm OD Telescope	3-21
4-1	Description of the Ray-Trace Axis Systems Used for All Reflective Detector Channels (3 Sheets)	4-4
4-2	Dimensional Parameters for Channel 1 (Reflective) (3 Sheets)	4-7
4-3	Dimensional Parameters for Channel 2 (Reflective) (3 Sheets)	4-10
4-4	Dimensional Parameters for Channel 3 (Reflective) (3 Sheets)	4-13
4-5	Dimensional Parameters for Channel 4 (Reflective) (3 Sheets)	4-16
4-6	Dimensional Parameters for Channel 11 (Reflective) (3 Sheets)	4-19
4-7	Dimensional Parameters for Channel 12 (Reflective) (3 Sheets)	4-22
4-8	Dimensional Parameters for Channel 13 (Reflective) (3 Sheets)	4-25
4-9	Description of the Ray-Trace Axis Systems Used for All Transmissive Detector Channels (3 Sheets)	4-29
4-10	Dimensional Parameters for Channel 5 (Transmissive) (3 Sheets)	4-32
4-11	Dimensional Parameters for Channel 6 (Transmissive) (3 Sheets)	4-35

LIST OF TABLES (continued)

TABLE NO.		PAGE
4-12	Dimensional Parameters for Channel 7 (Transmissive) (3 Sheets)	4-38
4-13	Dimensional Parameters for Channel 8 (Transmissive) (3 Sheets)	4-41
4-14	Dimensional Parameters for Channel 9 (Transmissive) (3 Sheets)	4-44
4-15	Dimensional Parameters for Channel 10 (Transmissive) (3 Sheets)	4-47
4-16	Dimensional Parameters for Channel 14 (Transmissive) (3 Sheets)	4-50
4-17	Summary of the Design and Performance of the Sixteen Detector Channels	4-53
4-18	Error Analysis for Channel 5 Detector Optical System (2 Sheets)	4-57
4-19	Error Analysis for Channel 4 Detector Optical System	4-59
4-20	Dimensional Tolerances for One-Percent Detector Image Error (Channels 4 and 4)	4-62
5-1	Dimensional Parameters for Toroidal Chopper for 61-mm OD Telescope	5-3
5-2	Dimensional Parameters for Toroidal Chopper for 80-mm OD Telescope	5-4

LIST OF ILLUSTRATIONS

FIGURE NO.		PAGE
3-1	Ray-Trace Axis System for the 80-mm OD Double-Sphere Telescope	3-5
3-2	Angular Field-of-View 200-Ray Diagrams for Ray Starting Points at Edge and Center of Field Stop	3-11
3-3	Ray-Trace Axis System Used for Error Analysis of 61-mm OD Double-Sphere Cassegrainian Telescope	3-16
3-4	Plot of Errors for 61-mm Telescope	3-20
4-1	Optical Schematic Showing Two Detector Optical Channels Following Each Telescope	4-2
4-2	Ray-Trace Axis Systems for Reflected Channel 11 and Transmitted Channel 8	4-3
4-3	Zones of Illumination on the Detector Surface	4-55
4-4	Channel 4 and 5 Error Analysis	4-61
5-1	3-View Ray-Trace Analysis of Toroidal Mirror for 61-mm OD Telescopes.	5-2
5-2	32-Ray Spot Diagram Showing Detector Image Size at Reference Blackbody Opening for Toroid Chopper for 61-mm OD Telescope	5-5

DETAILS OF TOVS-BSU OPTICAL DESIGN

1.0 INTRODUCTION

A detailed description of the final optical design is presented in this Appendix. This final optical design configuration was developed through the extensive use of computer ray-trace analyses to optimize radiant transfer efficiency, radiometric sensitivity and accuracy, and the long-term stability and reliability of the radiometer. Some of the features of this final optical design are these:

1. Up to eight separate Cassegrainian telescopes may be used to image the same angular field-of-view on circular field stops at each of their prime image planes. Four of the telescopes have a primary mirror diameter of roughly 80 mm, and the other four telescopes are optically scaled down to a primary mirror diameter of roughly 61 mm. A dichroic filter beamsplitter follows the field stop of each telescope and splits the radiation into two separate detector channels, and each detector channel consists of, in order, two spectral bandpass filters, a doublet lens, a window for sealing the detector, and finally the detector.

2. The primary and secondary mirrors of the Casegrainian telescopes have spherical surfaces. The optical aberrations produced by such a double-sphere form of Cassegrainian telescope are larger than those produced by several other forms of the Cassegrainian telescope. However, even though the optical aberrations are relatively large, the actual angular field-of-view radiant distribution function for this double-sphere telescope design meets the required field-of-view specifications. Further, the spherical mirror surfaces can be manufactured to high quality and accuracy considerably more economically than can aspheric mirror surfaces. Mirrors of high quality and accuracy are very necessary to obtain both the angular field-of-view matching between all the telescopes and the low level of stray radiation required by the specifications.

3. The secondary mirror of each telescope is made the aperture stop of its telescope by imaging it directly on the detectors of both channels which follow it by use of the doublet lens of each channel. The sensitive area of the detector is designed to be very slightly smaller than the secondary mirror image upon it. A perfect match between the secondary mirror image and the detector area would mean that the detector receives the maximum radiation from the telescope field-of-view, but does not receive any by-passing radiation from outside the secondary mirror. This optical design feature can insure that each of the radiometer channels will have very low stray-radiation levels. It also permits the secondary mirror to have a minimum physical diameter which increases the telescope acceptance area and reduces its diffraction aberrations.

4. The doublet lens of each detector channel represents the minimum number of lens elements that are practical. The individual optical elements of each of the doublet lenses have also been kept to a minimum thickness. Germanium lenses are used for channels 1 through 11, while silicon lenses are used for channels 12, 13, and 14.

5. A single rotating optical chopper disc serves all the telescopes. Its plane of rotation is located immediately before the field stops of each telescope. The chopper surface facing each field stop is a toroidal mirror which images both detectors which follow it into a blackbody reference cavity. A separate blackbody reference cavity is provided for each field stop and is located between the chopper and the field stop. These blackbody reference cavities require only a relatively small area opening in comparison to their internal surface area which insures a high emissivity. The field stops for the 80-mm telescopes are located on a different radius than the field stops for the 61-mm telescope; so the 80- and 61-mm telescopes actually use different toroidal surfaces. However, these two toroidal surfaces are part of the same chopper structure. Each toroid surface has four windows which are 180 degrees out of phase with each other, so each channel is provided with four chopping cycles per chopper rotation.

The optical ray-trace analysis which was used to develop and define the final optical design for this radiometer involves pure mathematical model-building techniques which permitted quick, accurate comparisons of all possible optical design approaches, and then permitted the optimization of the preferred design approach. Finally, the ray-trace analysis was used to define all of the optical element parameters, image characteristics, and tolerances for construction planning and for in-service error analysis.

2.0 RAY-TRACE DESCRIPTION

The computer ray-trace analyses which have been performed for this study are mathematical model-building procedures, wherein exact mathematical equations are used to express each optical surface and each light ray. Each optical surface is mathematically defined in a separate three-dimensional axis-system which may have any linear or angular orientation to the previous axis-system, and the light rays may have any orientation to the axis-systems. All mathematical calculations are exact, and no mathematical approximations are required. All the ray-trace computations are performed by an IBM 360 Model 65 Computer in double precision. The computed coordinate accuracy for each ray-surface intercept in its three-dimensional axis-system is given to an accuracy of 10^{-8} mm, and the computed direction cosine accuracy for each ray in its three-dimensional axis-system is given to an accuracy of 10^{-8}.

Table 2-1 defines the dimensional parameters which are required by every ray-trace, which transform axis systems, describe surface shapes, etc. Table 2-2 defines the coordinates of the resultant ray-surface intercepts and gives the terminology used for an image analysis at any surface. Table 2-3 defines the three-direction cosines of the rays at the resultant ray-surface intercepts and gives the terminology used for an angular image analysis. The "mathematical axis systems," which are occasionally used, facilitate only in defining the orientation and location of the next optical surface.

TABLE 2-1 (SHEET 1 of 2). DEFINITIONS FOR RAY-TRACE DIMENSIONAL PARAMETERS

The following coefficients define each optical surface in its own axis system, and define its own axis system relative to the previous axis system:

I. Each successive optical surface in an optical system is defined by a separate three-dimensional, right-handed axis system (X_n, Y_n, Z_n) which carries a progressive set of subscripts which run from 1 to m, where m is the number of the surface being ray-traced, and the following dimensional parameters define the linear and the rotational axis transformations from the $(X_{n-1}, Y_{n-1}, Z_{n-1})$ axis system of the previous optical surface to the (X_n, Y_n, Z_n) axis system of the surface being ray-traced:

A_n The X_{n-1} coordinate for the origin of the (X_n, Y_n, Z_n) axis system measured in the $(X_{n-1}, Y_{n-1}, Z_{n-1})$ axis system.

B_n The Y_{n-1} coordinate for the origin of the (X_n, Y_n, Z_n) axis system measured in the $(X_{n-1}, Y_{n-1}, Z_{n-1})$ axis system.

C_n The Z_{n-1} coordinate for the origin of the (X_n, Y_n, Z_n) axis system measured in the $(X_{n-1}, Y_{n-1}, Z_{n-1})$ axis system.

α_n The angular displacement of the X_n-axis in the X_n-Z_n plane, which is positive when the positive X_n-axis is moved toward the positive Z_n-axis, and negative when the positive X_n-axis is moved toward the negative Z_n-axis.

β_n The angular displacement of the X_n-axis in the X_n-Y_n plane, which is positive when the positive X_n-axis is moved toward the positive Y_n-axis, and negative when the positive X_n-axis is moved toward the negative Y_n-axis.

TABLE 2-1 (SHEET 2 of 2). DEFINITIONS FOR RAY-TRACE DIMENSIONAL PARAMETERS

γ_n The angular displacement of the Z_n-axis in the Y_n-Z_n plane, which is positive when the positive Z_n-axis is moved toward the positive Y_n-axis, and negative when the positive Z_n-axis is moved toward the negative Y_n-axis.

The three angular transformations, α_n, β_n, γ_n are operative only after the linear transformations, A_n, B_n, C_n have been completed. The three angular transformations may be defined in any order, but each transformation must be completed before the next becomes operative.

II. The dimensional parameters F_n, D_n, E_n, and R_n may define any conic surface, since they are the coefficients of the following general equation:

$$F_n X_n^2 + D_n Y_n^2 + E_n Z_n^2 - 2R_n X_n = 0$$

III. A plane optical surface is always the Y_n-Z_n plane.

IV. N_n The index of refraction of the optical medium immediately following the optical surface which is defined in the (X_n, Y_n, Z_n) axis system.

TABLE 2-2 (SHEET 1 of 2). DEFINITIONS FOR THE RESULTANT RAY-SURFACE INTERCEPTS AND THE TERMINOLOGY FOR THE RESULTANT LATERAL IMAGE CHARACTERISTICS

X_n	The X_n coordinate of a single ray intercept with the optical surface in the (X_n, Y_n, Z_n) axis system.
Y_n	The Y_n coordinate of a single ray intercept with the optical surface in the (X_n, Y_n, Z_n) axis system.
Z_n	The Z_n coordinate of a single ray intercept with the optical surface in the (X_n, Y_n, Z_n) axis system.
D_n	The optical distance a single ray travels between two successive surfaces. This is defined as the true distance between the ray-intercepts $(X_{n-1}, Y_{n-1}, Z_{n-1})$ and (X_n, Y_n, Z_n) multiplied by N_{n-1}.
Centroid X_n	The mathematical centroid for the X_n values for all rays from a single family of rays.
Centroid Y_n	The mathematical centroid for the Y_n values for all rays from a single family of rays.
Centroid Z_n	The mathematical centroid for the Z_n values for all rays from a single family of rays.
ΔX_n	The maximum mathematical difference for all X_n values for a single family of rays.
ΔY_n	The maximum mathematical difference for all Y_n values for a single family of rays.

TABLE 2-2 (SHEET 2 of 2). DEFINITIONS FOR THE RESULTANT RAY-SURFACE INTERCEPTS AND THE TERMINOLOGY FOR THE RESULTANT LATERAL IMAGE CHARACTERISTICS

ΔZ_n	The maximum mathematical difference for all Z_n values for a single family of rays.
$75\% \Delta X_n$	The smallest maximum mathematical difference for any 75% of the X_n values from a single family of rays. This is an approximation for the half-power spread for all the X_n values of the family of rays.
$75\% \Delta Y_n$	The smallest maximum mathematical difference for any 75% of the Y_n values from a single family of rays. This is an approximation for the half-power spread for all the Y_n values of the family of rays.
$75\% \Delta Z_n$	The smallest maximum mathematical difference for any 75% of the Z_n values from a single family of rays. This is an approximation for the half-power spread for all the Z_n values of the family of rays.

TABLE 2-3 (SHEET 1 of 2). DEFINITIONS FOR THE RESULTANT RAY DIRECTION COSINES AND THE TERMINOLOGY FOR THE RESULTANT ANGULAR IMAGE CHARACTERISTICS

Xi_n	The direction cosine component on the X_n-axis for a ray departing from the ray-surface intercept of the (X_n,Y_n,Z_n) axis system.
Eta_n	The direction cosine component on the Y_n-axis for a ray departing from the ray-surface intercept of the (X_n,Y_n,Z_n) axis system.
$Zeta_n$	The direction cosine component on the Z_n-axis for a ray departing from the ray-surface intercept of the (X_n,Y_n,Z_n) axis system.
Centroid Xi_n	The mathematical centroid for the Xi_n values for all rays from a single family of rays.
Centroid Eta_n	The mathematical centroid for the Eta_n values for all rays from a single family of rays.
Centroid $Zeta_n$	The mathematical centroid for the $Zeta_n$ values for all rays from a single family of rays.
ΔXi_n	The maximum mathematical difference for all Xi_n values for a single family of rays.
ΔEta_n	The maximum mathematical difference for all Eta_n values for a single family of rays.

TABLE 2-3 (SHEET 2 of 2). DEFINITIONS FOR THE RESULTANT RAY DIRECTION COSINES AND THE TERMINOLOGY FOR THE RESULTANT ANGULAR IMAGE CHARACTERISTICS

$\Delta Zeta_n$	The maximum mathematical difference for all $Zeta_n$ values for a single family of rays.
$75\% \Delta Xi_n$	The smallest maximum mathematical difference for any 75% of the Xi_n values from a single family of rays. This is an approximation for the half-power spread for all the Xi_n values of the family of rays.
$75\% \Delta Eta_n$	The smallest maximum mathematical difference for any 75% of the Eta_n values from a single family of rays. This is an approximation for the half-power spread for all the Eta_n values of the family of rays.
$75\% \Delta Zeta_n$	The smallest maximum mathematical difference for any 75% of the $Zeta_n$ values from a single family of rays. This is an approximation for the half-power spread for all the $Zeta_n$ values of the family of rays.
	Note: When the direction cosine values are sufficiently small, they may be dimensioned as radian values.

3.0 TELESCOPE DESIGN

3.1 Telescope Requirements

The radiometer can use up to eight Cassegrainian telescopes, each of which meets the following angular field-of-view performance specifications:

Description of Specification	Angular Diameter of a Circular Field-of-View
The half-power angular field-of-view diameter for each of the 14 channels shall be less than	1.200 degrees (maximum) 1.125 degrees (goal)
99% of the radiation received by each channel must arrive from within an angular field-of-view diameter of	1.250 degrees
The radiometric energy centroid for the measured angular field-of-view diameter for each of the other channels shall match that of channel 4 within	1 percent of the angular field-of-view diameter for channel 4

3.2 Choice of Telescope Type

A form of Cassegrainian telescope has been selected for this radiometer, since the physical length of a Cassegrainian telescope can be considerably shorter than its focal length. A long focal length telescope expands the image of the small 1.125-degree angular field-of-view sufficiently to be defined by a reasonably-sized field stop for the filters and the detector lenses. The most

common type of Cassegrainian telescope uses a paraboloid primary mirror and a hyperboloid secondary mirror. Such a telescope, theoretically, has zero optical aberrations on its optical axis for an object at infinity, but aberrations increase as the field-of-view angle is increased from 0 degree. Other types of Cassegrainian telescopes use ellipsoidal or other higher-degree aspheric surfaces for the primary and/or the secondary mirrors.

The most economical type of Cassegrainian telescope to construct is, certainly, one using spherical mirror surfaces for both the primary and secondary mirrors. The optical aberrations on the optical axis for such a double-sphere Cassegrainian telescope are too large for many applications, but these already-large aberrations on the optical axis increase only very slightly with increased field-of-view angle. The TOVS-BSU radiometer does not require any specific image resolution capability within its field-of-view. The actual half-power angular aberrations for the double-sphere Cassegrainian telescope under investigation, it turns out, are sufficiently small that both the specified half-power angular field-of-view and the 99-percent radiation field-of-view diameter are met. For these reasons, the double-sphere Cassegrainian telescope has been selected for final design study.

3.3 A Comparative Analysis of a Double-Sphere Cassegrainian Telescope and a Paraboloid-Hyperboloid Cassegrainian Telescope

A comparative analysis of the angular field-of-view aberrations in object space was performed for the ITPR double-sphere Cassegrainian telescope vs. a paraboloid-hyperboloid Cassegrainian telescope for the ITPR telescope design study[1]. The two telescopes have roughly the same numerical aperture and focal length, and 100-ray families were traced from starting points both at the center and the edge of their field stops to object space. Each family of rays intersected its telescope secondary mirror, making it the telescope aperture stop in a uniform area array. The angular field-of-view spread

[1]Optical Analysis Report, by B.D. Henderson, Contract No. E-80-70-N, Nov. 1970

characteristics for each 100 rays were then analyzed in object space. Table 3-1 shows these results using the nomenclature defined in Table 2-3. It is seen that the paraboloid-hyperboloid telescope is still ten-fold better at the edge of the field-of-view than the ITPR double-sphere telescope. However, the double-sphere aberrations are considerably less than the centroid Eta_3 value, the angular radius of the field-of-view.

3.4 Dimensional Parameters for the 80- and 61-mm OD TOVS-BSU Telescopes

Figure 3-1 is an accurate computer plot of selected rays, which include the four telescope boundary rays in the X-Y plane, traced through the 80-mm OD double-sphere telescope. The axis systems shown in Figure 3-1 were used to ray-trace both the 80- and 61-mm OD telescopes. Table 3-2 describes the optical elements which are spacially located by each axis system of Figure 3-1. Tables 3-3 and 3-4 list the dimensional parameters for the 80- and 61-mm OD telescopes, respectively. The definitions for the nomenclature used in Tables 3-2, 3-3, and 3-4 are found in Table 2-1.

3.5 Angular Field-of-View Image Characteristics for the 61- and 80-mm OD Telescopes

A computer ray-trace analysis was performed to determine the quality of the angular field-of-view image for the 61- and 80-mm OD telescopes in object space. This ray trace started from points both at the center and at the edge of the field stop of each telescope. A family of 200 rays was traced from each of these starting points. Each family of 200 rays intercepted its telescope secondary mirror in precisely the same uniform area circular array of points, which fill the diameter of the secondary mirror. Such a ray-pattern selection makes the secondary mirror the aperture stop of the telescope since the same area of the secondary mirror is used for all field-of-view angles.

Each family of 200 rays was ray-traced from its starting points on the field stop to, successively, the secondary mirror, the primary mirror, and finally the Y_3-Z_3 plane in object space. The angular field-of-view aberrations for each family of 200 rays were analyzed by using the eta_3 and $zeta_3$ direction cosines in the (X_3,Y_3,Z_3) axis system. Since the ray angles about the X_3-axis are small, the Eta_3 and $Zeta_3$ values are numerically equivalent to radian units for most practical purposes.

TABLE 3-1. COMPARATIVE ANGULAR FIELD-OF-VIEW CHARACTERISTICS FOR THE ITPR DOUBLE-SPHERE CASSEGRAINIAN TELESCOPE, AND A PARABOLOID-HYPERBOLOID CASSEGRAINIAN TELESCOPE OF THE SAME SIZE

Type of Cassegrainian Telescope	Starting Point is Center of Field Stop				Starting Point is Edge of Field Stop on Y_o-axis			
	Centroid Eta_3	ΔEta_3	$\Delta Zeta_3$	75% ΔEta_3	Centroid Eta_3	ΔEta_3	$\Delta Zeta_3$	75% ΔEta_3
Paraboloid-Hyperboloid	0	0	0	0	.01239	.0003	.0002	.00012
Double-Sphere	0	.00271	.00257	.00164	.01288	.00291	.00266	.00193

Note: All values are in direction cosine units; however, for these small magnitudes, they may also be taken as radian units.

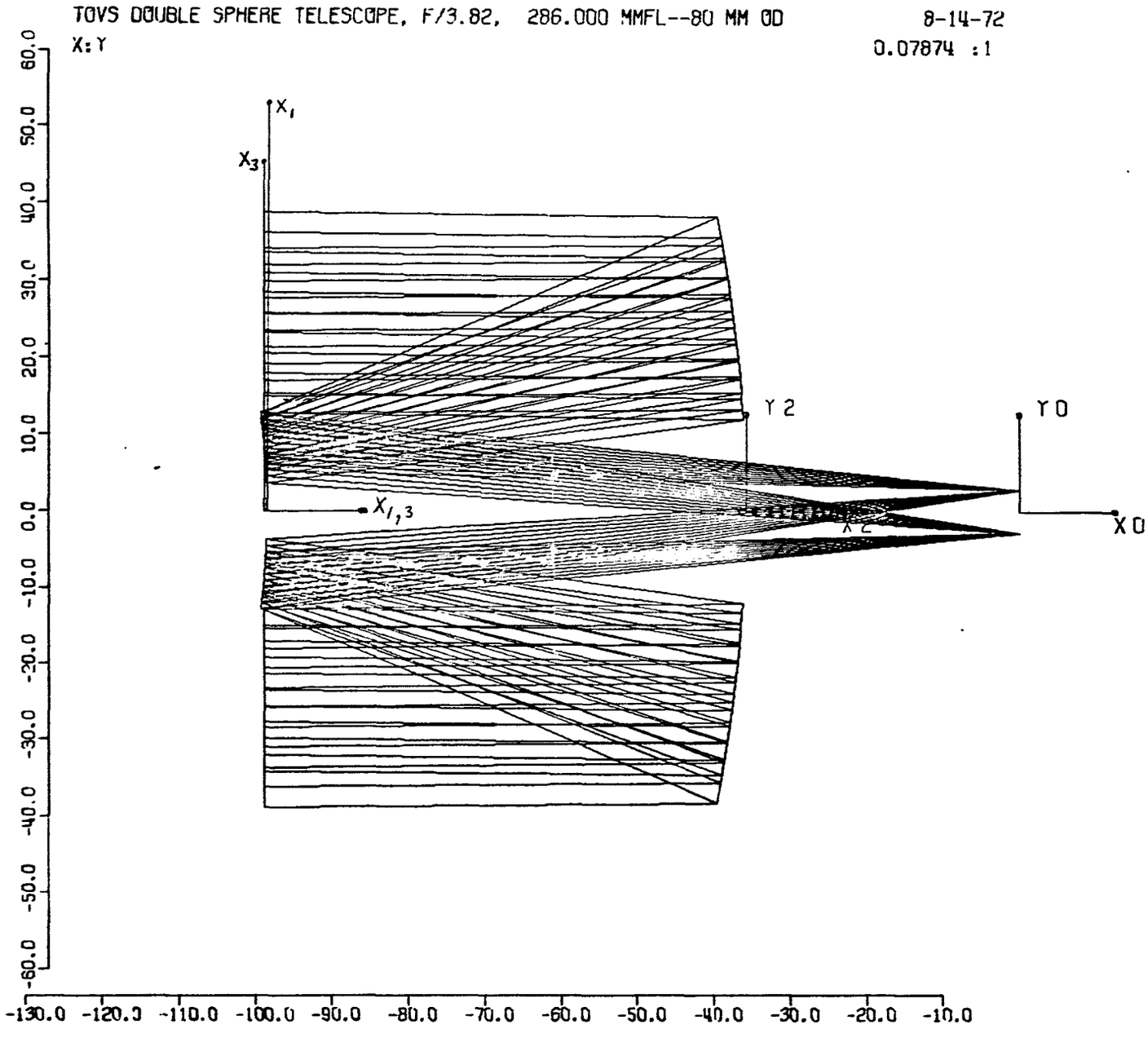

Figure 3-1. Ray-Trace Axis System for the 80-mm OD Double-Sphere Telescope

TABLE 3-2. DESCRIPTION OF THE RAY-TRACE AXIS SYSTEMS FOR BOTH THE 80- AND 61-MM OD DOUBLE-SPHERE CASSEGRAINIAN TELESCOPES

The same axis systems are used to ray-trace both the 80- and 61-mm OD double-sphere Cassegrainian telescopes. Ray-trace starting points are located on the field stop, and the rays are traced to, successively, the secondary mirror, primary mirror, and then to object space.

(X_o,Y_o,Z_o)	Field Stop: the field stop lies in the Y_o-Z_o plane.
(X_1,Y_1,Z_1)	Secondary Mirror: this mirror has a reflecting spherical surface. Its apex is at the origin of the (X_1,Y_1,Z_1) axis system, and its center lies on the negative X_1-axis.
(X_2,Y_2,Z_2)	Primary Mirror: This mirror has a reflecting spherical surface. Its apex is at the origin on the (X_2,Y_2,Z_2) axis system, and its center lies on the negative X_2-axis.
(X_3,Y_3,Z_3)	Image Plane: this is a transmitting plane surface in the Y_3-Z_3 plane. It is used to measure both ray positions and the ray direction cosines in object space.

TABLE 3-3. DIMENSIONAL PARAMETERS FOR 80 MM OD TELESCOPE

Axis Sub-Script (n)	Optical Function of Surface	A_n (mm)	B_n (mm)	C_n (mm)	α_n (deg)	β_n (deg)	γ_n (deg)	Surface Shape	D_n (mm)	E_n (mm)	F_n (mm)	R_n (mm)	N_n (mm)
1	Secondary Mirror	-98.440						Sphere	1.0	1.0	1.0	-103.200	1.0000
2	Primary Mirror	62.600						Sphere	1.0	1.0	1.0	-194.500	1.0000
3	Image Plane	-63.000						Plane					1.0000

TABLE 3-4. DIMENSIONAL PARAMETERS FOR 61 MM OD TELESCOPE

Axis Sub-Script (n)	Optical Function of Surface	A_n (mm)	B_n (mm)	C_n (mm)	α_n (deg)	β_n (deg)	γ_n (deg)	Surface Shape	D_n (mm)	E_n (mm)	F_n (mm)	R_n (mm)	N_n (mm)
1	Secondary Mirror	-74.860						Sphere	1.0	1.0	1.0	-78.700	1.000
2	Primary Mirror	47.700						Sphere	1.0	1.0	1.0	-148.200	1.000
3	Image Plane	-48.000						Plane					1.0000

Table 3-5 summarizes the resultant angular field-of-view aberration characteristics for the 80- and 61-mm OD telescopes. Table 2-3 defines the terminology used for the angular image analysis in Table 3-5. The centroid Eta_3 values of Table 3-5 are, of course, zero when the starting point is $Y_o = 0$, the center of the field stop. The centroid $Zeta_3$ values are not given because they are always zero, since $Z_o = 0$ for both the center and edge of the field starting points. The angular field-of-view aberration characteristics for the ITPR double-sphere telescope, shown in Table 3-1, are roughly the same magnitude as those for TOVS-BSU shown in Table 3-5. The difference is due to the larger angular field-of-view for the ITPR telescopes, 1.250 degrees.

Figure 3-2 shows the spot diagrams for the two families of rays for both the 80- and 61-mm OD telescopes. These angular field aberrations are identical for both the 80- and 61-mm OD telescope.

In operation, only the image quality at the defining edge of the field stop is of importance to the radiometer, so only those aberration values for the edge of the field stop should be considered. The centroid Eta_3 value for both the 80-mm OD telescope when $Y_o = 2.815$ and $Z_o = 0$, and for the 61-mm OD telescope when $Y_o = 2.141$ and $Z_o = 0$, is

$$0.00977 \text{ radians} \times \frac{180 \text{ degrees}}{\pi} = 0.560 \text{ degree}$$

The half-power angular field-of-view for the full field stop diameter is then

$$0.560 \text{ degree} \times 2 = 1.120 \text{ degrees}$$

This is within the desired 1.125-degree maximum half-power angular field-of-view. Now, the maximum angular aberration spread for all Eta_3 values is

$$0.0109 \text{ radians} \times \frac{180 \text{ degrees}}{\pi} = 0.624 \text{ degree},$$

and the maximum angular spread for all rays is then

$$0.624 \text{ degree} \times 2 = 1.248 \text{ degrees}$$

TABLE 3-5. ANGULAR FIELD-OF-VIEW CHARACTERISTICS FOR THE 80- AND 61-MM OD DOUBLE-SPHERE CASSEGRAINIAN TELESCOPES

	Starting Point $Y_o = 0$; $Z_o = 0$				Starting Point $Y_o = -2.815$; $Z_o = 0$ (80-mm OD) $Y_o = -2.141$; $Z_o = 0$ (61-mm OD)			
TOVS-BSU Cassegrainian Telescope	Centroid Eta_3	ΔEta_3	$\Delta Zeta_3$	75% ΔEta_3	Centroid Eta_3	ΔEta_3	$\Delta Zeta_3$	75% ΔEta_3
80-mm OD	0	0.00208	0.00208	0.00142	0.00977	0.00286	0.00222	0.00135
61-mm OD	0	0.00208	0.00208	0.00142	0.00977	0.00287	0.00222	0.00135

Note: All values are in direction cosine units; however, for these small magnitudes, they may also be taken as radian units. Y_o and Z_o values are in millimeters (mm).

TOVS DOUBLE SPHERE TELESCOPE, F/3.82, 286.709 MMFL--80 MM OD 8-14-72

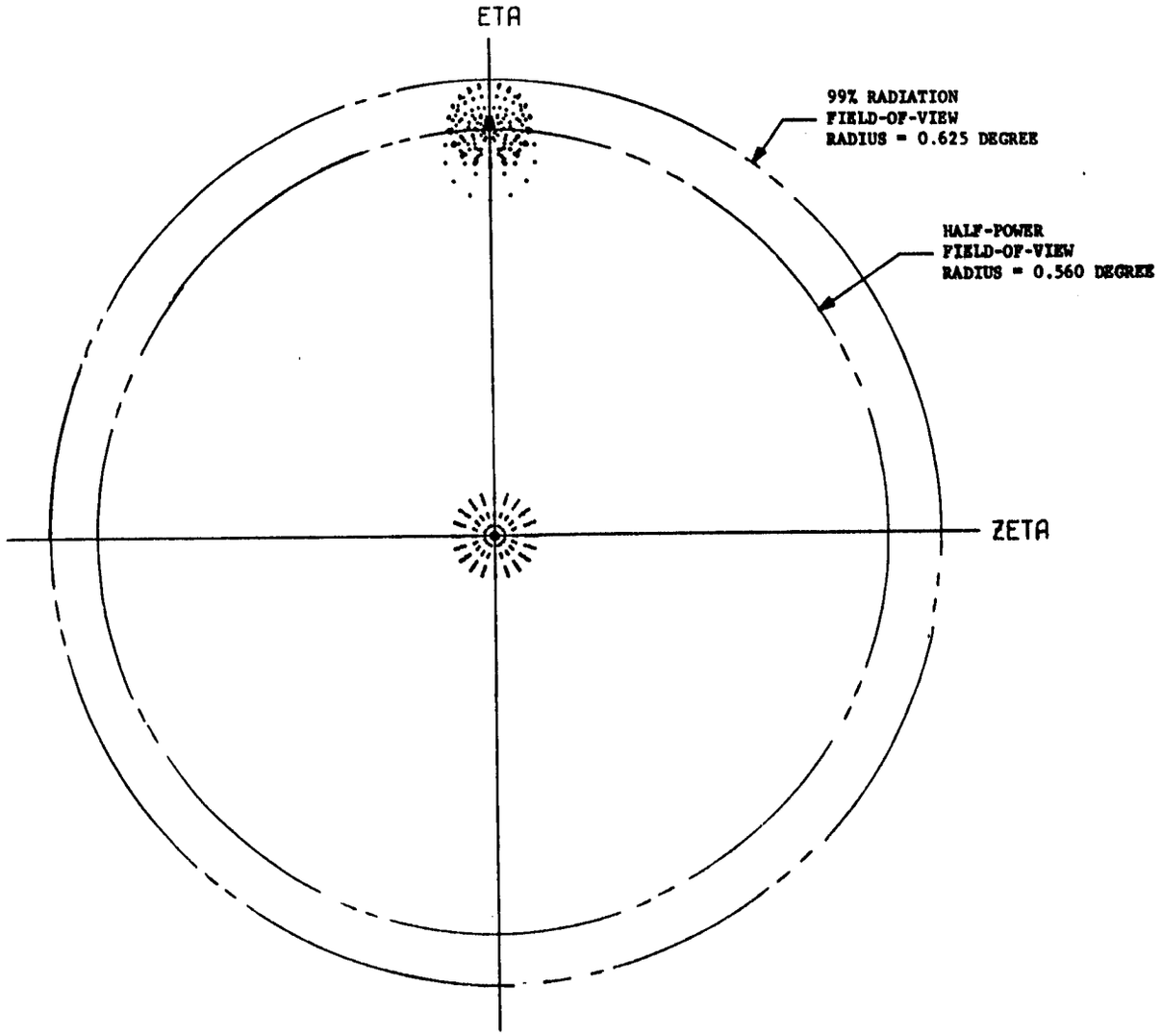

					MAX	MIN	
ZETA	HALF AXIS LENGTH	0.01200	ZETA	=	0.0011	-0.0011	SURFACE NO.
ETA	HALF AXIS LENGTH	0.01200	ETA	=	0.0109	0.0081	3

Figure 3-2. Angular Field-of-View 200-Ray Diagrams for Ray Starting Points at Edge and Center of Field Stop

Thus, the total field-of-view for all rays passing through the field stop, including the rays with the maximum optical aberrations, is within the 1.250 degrees for which more than 99 percent of the radiant flux must arise. This ray-trace analysis, however, has ignored the image aberrations due to diffraction, which will cause a small percentage of the rays to pass through the field stop which arrive from outside a 1.250-degree field-of-view. This will occur mostly for the long wavelength channel 14.

The foregoing image analysis shows that both the 80- and 61-mm OD double-sphere Cassegrainian telescopes can meet the angular field-of-view requirements for this radiometer. Furthermore, there is no need for better angular resolution within the field-stop area, since the only purpose of each radiometer channel is to measure the spectral radiant flux that passes through its field stop.

3.5 The 80- and 61-mm OD Double-Sphere Telescope Specifications

The dimensions and optical performance characteristics for the 80- and 61-mm OD double-sphere telescopes are given along with those for the ITPR telescope in Table 3-6.

3.6 Light Shield for a Cassegrainian Telescope

A tubular light shield is usually positioned between the primary and secondary mirrors of a Cassegrainian telescope, and supported by, or through, the hole in the primary mirror. This light shield prevents light bypassing the primary and secondary mirrors and falling directly on the prime focal plane of the telescope. Such a light shield is necessary when photography or photometry is performed at the prime focus of the telescope. Without this shield, the telescope image is washed out or reduced in contrast by the background illumination.

To make a light shield effective, the secondary mirror must generally be larger in diameter than is needed to produce the required field-of-view. This increase in size of the secondary mirror reduces optical efficiency and increases diffraction effects.

TABLE 3-6. TOVS-BSU AND ITPR DOUBLE-SPHERE TELESCOPE SPECIFICATIONS

		TOVS 61-mm OD	TOVS 80-mm OD	ITPR
Primary Mirror Radius of Curvature	(mm)	148.20	194.50	121.6073
Secondary Mirror Radius of Curvature	(mm)	78.70	103.20	64.5231
Primary-Secondary Mirror Spacing	(mm)	47.70	62.60	39.100
Secondary Mirror-Field-Stop Spacing	(mm)	74.86	98.44	61.100
Secondary Mirror OD	(mm)	19.52	25.60	16.000
Primary Mirror OD	(mm)	61.0	80.0	53.249
Primary Mirror Used Area OD	(mm)	58.452	76.654	45.708
Focal Length	(mm)	218.062	286.709	178.571
Field Stop Diameter	(mm)	4.282	5.630	4.6
Half-Power Angular Field-of-View Diameter (Diffraction Neglected)	(°)	1.120	1.120	1.4760
Numerical Aperture (NA) at Field Stop, Neglecting Light Obscuration		0.131* 0.128**	0.131* 0.128**	0.131* 0.129*
Relative Aperture at Field Stop, Neglecting Light Obscuration		f/3.84	f/3.84	f/3.82
Total Area of Acceptance, Neglecting Obscuration	(cm^2)	24.40	41.85	16.4087
Area of Obscuration by Secondary Mirror	(cm^2)	2.99	5.15	2.0106
Area of Obscuration by the Three Spiders	(cm^2)	.54	.71	0.4456
Total Area of Obscuration	(cm^2)	3.53	5.86	2.4562
Total Area of Acceptance, Including Losses of Spider and Secondary Mirror	(cm^2)	20.87	35.99	13.9525
Percent Obscuration	(%)	14.46	14.00	14.95

* For image at center of field-of-view
** For image at edge of field-of-view

Such tubular light shields are not necessary for the TOVS-BSU telescopes because photodetection is not performed at the prime focus of the telescopes, which is the location of the field stop. Detector lenses are positioned after each telescope field stop to image the telescope secondary mirror directly on the detector sensitive area. The outside diameter of the detector is just slightly smaller than the diameter of the image of the secondary mirror. This means that all those rays which bypass the telescope primary and secondary mirrors and pass directly through the field stop will be imaged outside of the outer diameter of the sensitive detector area.

This method of controlling stray light by "image control" is generally more effective in a compound optical system such as used in this radiometer than are baffles and shields. Of course, in a simple optical system which has but a single image, baffles are usually a necessity for stray light control.

3.7 Dimple in Center of Telescope Secondary Mirror

A spherical concave dimple is ground and polished into the central portion of all telescope secondary mirrors. This dimple is accurately located to cover that zone of its own blockage of entering rays. The radii of these dimples is exactly equal to the spacing between the secondary mirror and the field stop, that is,

Dimple Radius = 98.44 mm for the 80-mm OD telescopes,
Dimple Radius = 74.86 mm for the 61-mm OD telescopes.

The dimple reimages the field stop on itself, and for the detector design which is used the detector image is returned to itself by the dimple mirror. This means the detector can receive chopped thermal radiation from the filters and lenses of the detector optical system. Therefore, it is necessary that these elements have only a very small temperature change between calibration cycles.

3.8 Error Analysis for the Double-Sphere Telescopes

The purpose of this error analysis is to gain an understanding of the manufacturing and assembly tolerances which are necessary or desirable for the

TOVS-BSU telescopes. Only the 61-mm OD telescope was ray-traced for the error analysis since it is a dimensionally smaller system and, thus, its performance characteristics will be more affected by a given mechanical tolerance.

Figure 3-3 shows the ray-trace axis system and two starting rays, which were used repeatedly for different error conditions within the telescope. This axis system defines this same telescope as defined by Figure 3-1 and Table 3-4, but in the reverse direction. Table 3-7 defines the dimensional parameters for this error analysis.

The two rays are parallel and arrive from a half-angular field-of-view of 0.5625 degree and are imaged near the edge of the field stop. These rays travel completely in X-Y planes of each axis system for each error analysis. Therefore, the two-ray image is at $Z_3 = 0$ at all times.

Table 3-8 describes the error performance of the 61-mm OD telescope for fifteen different error conditions, besides its zero error condition. In order to gain an understanding of how each type of error can affect the telescope focus (longitudinal error) and its lateral image position (lateral error), only one type and magnitude of error is inserted into the telescopes dimensional parameters at a time. Then a ray-trace is made with the same two-input rays. With each ray trace, the computor automatically adjusts A_3, the spacing between the secondary mirror and the field stop until the two rays precisely focus on the Y_3-Z_3 plane, or just the Y_3-axis, since $Z_3 = 0$ for this study. Table 3-8 gives the focused A_3 and Y_3 values for the zero error and the fifteen other error conditions. The columns following both A_3 and Y_3 show the change in that parameter relative to its zero error magnitude.

The types of errors described in Table 3-8 are the spacing between the primary and secondary mirrors, A_2; lateral shifts of one spherical mirror relative to the next surface, B_1, B_2, and B_3; and changes in spherical mirror radii, R_1 and R_2. Each type of error was ray-traced for three different magnitudes, covering two decades, 0.0025 mm, 0.0250 mm, and 0.250 mm, which are roughly equivalent, respectively, to 0.0001 inch, 0.0010 inch, and 0.0100 inch.

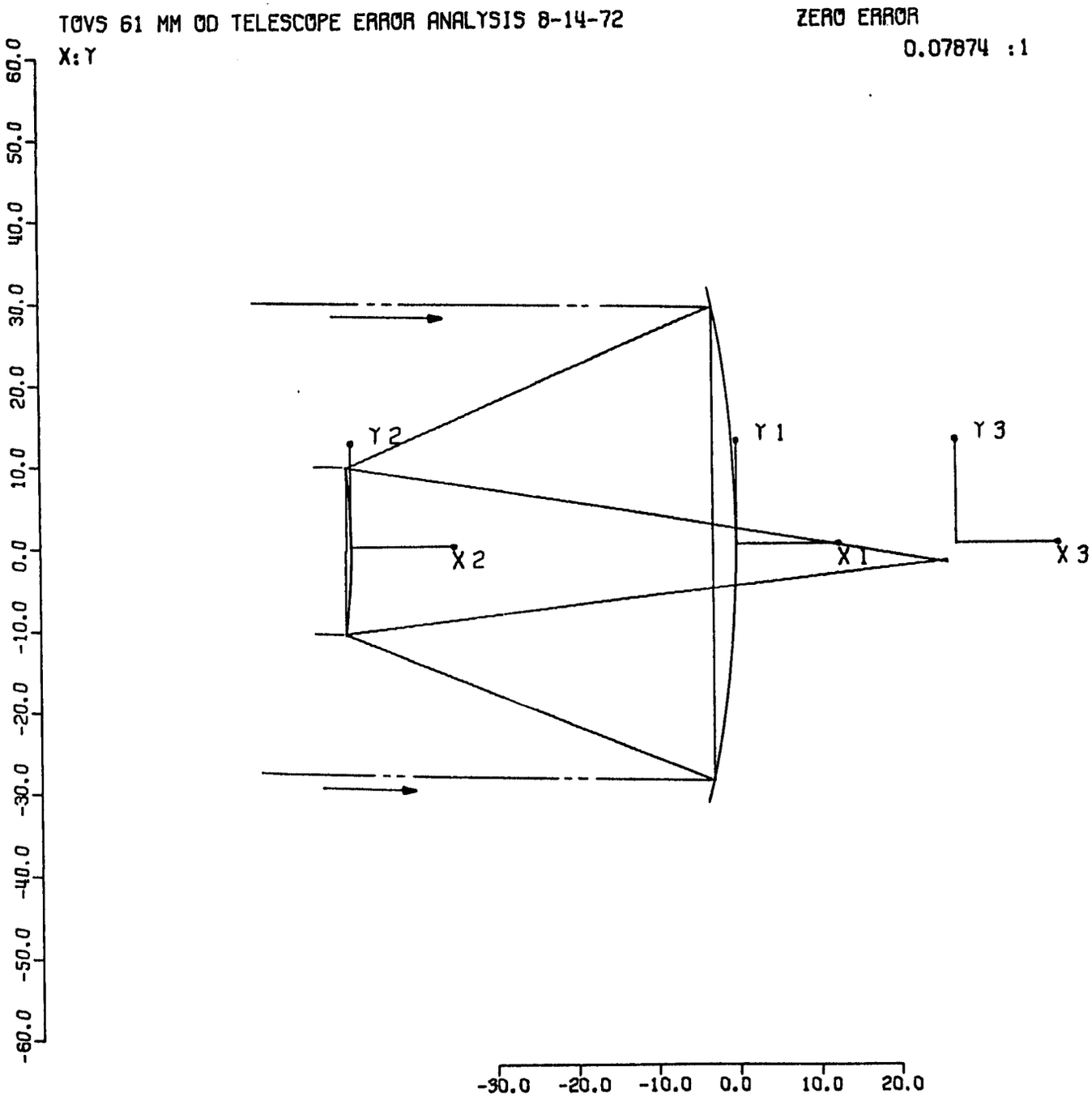

Figure 3-3. Ray-Trace Axis System Used for Error Analysis of 61-mm OD Double-Sphere Cassegrainian Telescope

TABLE 3-7. DIMENSIONAL PARAMETERS FOR 61 MM OD TELESCOPE ERROR ANALYSIS

Axis Sub-Script (n)	Optical Function of Surface	A_n (mm)	B_n (mm)	C_n (mm)	α_n (deg)	β_n (deg)	γ_n (deg)	Surface Shape	D_n (mm)	E_n (mm)	F_n (mm)	R_n (mm)	N_n (mm)'
1	Primary Mirror	100.000						Sphere	1.0	1.0	1.0	-148.20	1.0000
2	Secondary Mirror	-47.700						Sphere	1.0	1.0	1.0	-78.70	1.0000
3	Field Stop	74.860						Plane					1.0000

TABLE 3-8. ERROR ANALYSIS FOR 61-MM TELESCOPE

Code	Description	A_3	(O)-(N) ΔA_3	Y_3	(O)-(N) ΔY_3
0	Zero Error	72.696970		-2.175992	
1	A_2 = -47.6975	72.717747	-0.020777	-2.176381	0.000389
2	A_2 = -47.6750	72.905086	-0.208116	-2.179887	0.003895
3	A_2 = -47.500	74.813190	-2.116220	-2.215600	0.039608
4	B_1 = 0.0025, B_2 = -0.0025	72.697316	-0.000346	-2.168949	-0.007043
5	B_1 = 0.0250, B_2 = -0.0250	72.700806	-0.003836	-2.105566	-0.070426
6	B_1 = 0.2500, B_2 = -0.2500	72.728710	-0.031740	-1.471478	-0.704514
7	B_2 = 0.0025, B_3 = -0.0025	72.696803	0.000167	-2.180365	0.004373
8	B_2 = 0.0250, B_3 = -0.0250	72.695263	0.001707	-2.219723	0.043731
9	B_2 = 0.2500, B_3 = -0.2500	72.676167	0.020803	-2.613198	0.437206
10	R_1 = -148.1975	72.686543	0.010427	-2.175763	-0.000229
11	R_1 = -148.1750	72.592789	0.104181	-2.173707	-0.002285
12	R_1 = -147.9500	71.663662	1.033308	-2.153328	-0.022664
13	R_2 = - 78.6975	72.701240	-0.004270	-2.176116	0.000124
14	R_2 = - 78.6750	72.739704	-0.042734	-2.177236	0.001244
15	R_2 = - 78.4500	73.127795	-0.430825	-2.188534	0.012542

Figure 3-4 is a plot of all the errors from Table 3-8. Its log-log presentation of parameter error magnitude versus ΔA_3 and ΔY_3 shows that all of the errors are nearly linear over two decades. Thus, different types of error values, ΔA_3 or ΔY_3, may be either added to, or subtracted from, each other.

Figure 3-4 is now used to define the tolerance that may be placed on each parameter error. Two horizontal lines are drawn on Figure 3-4--one at a ΔY_3 value of 0.0428 mm, which is 1 percent of the diameter of the field stop, and the other at ΔA_3 value of 0.1712 mm, which represents a blur circle due to defocusing of the f/4 telescope image equal to 1 percent of the field stop diameter.

Table 3-9 lists, now, the error magnitude for the intersection of each of the two decade error plots with the respective 1-percent ΔA_3 (focal error), and 1-percent ΔY_3 (lateral error) lines on Figure 3-4. Table 3-9 shows the resultant errors in both mm and inches. Some of the errors are >0.25-millimeter or >0.0100 inch. This means these will have very little effect on focal or lateral image errors. On the other hand, a lateral shift of B_1 = 0.0151 mm or 0.0006 in. is sufficient to produce a 1-percent lateral field stop error, and B_2 is nearly as sensitive.

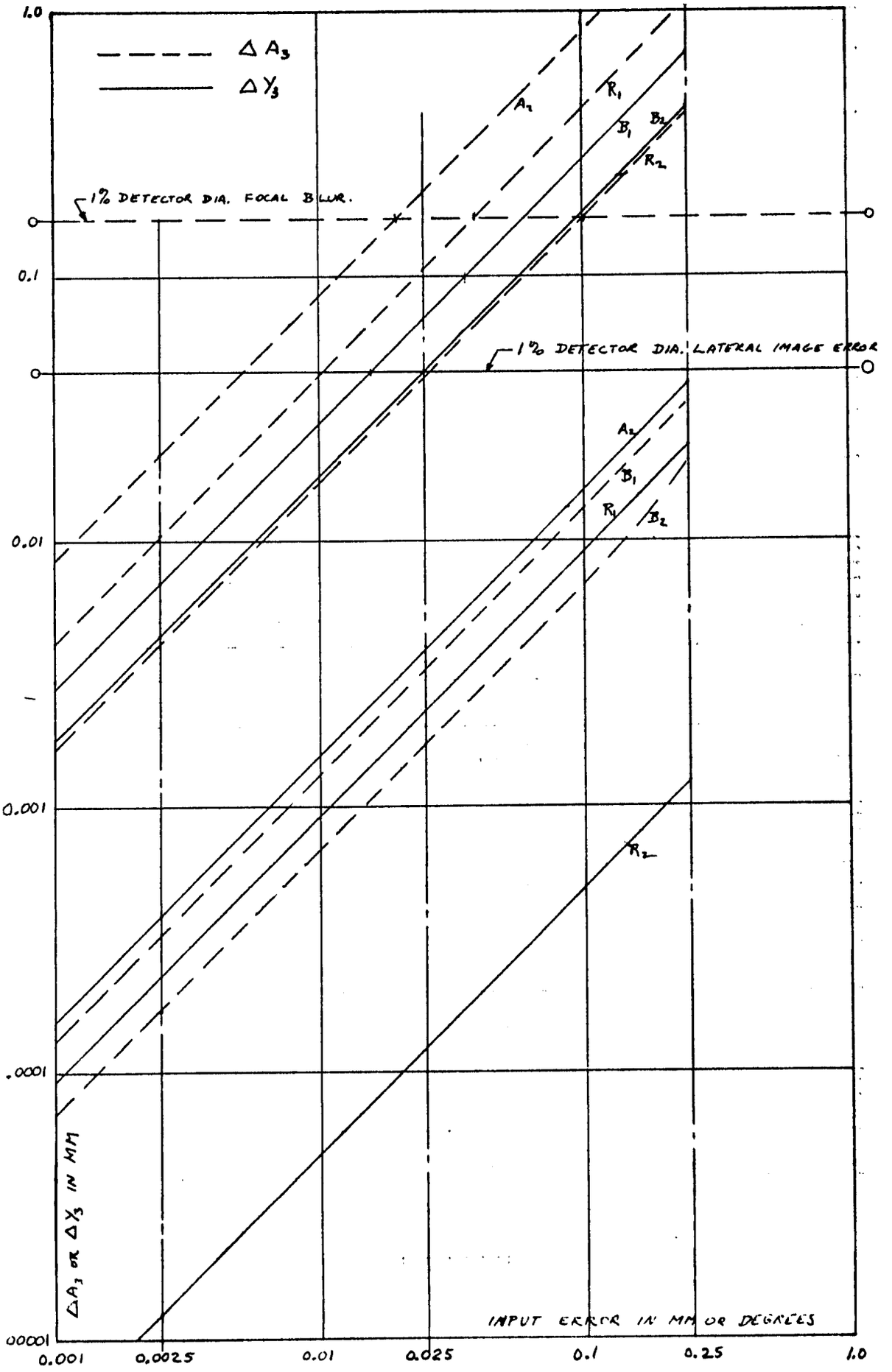

Figure 3-4. Plot of Errors for 61-mm Telescope

TABLE 3-9. DIMENSIONAL TOLERANCES FOR ONE-PERCENT FIELD STOP ERROR FOR 61-mm OD TELESCOPE

DESCRIPTION	FOCAL ERROR		LATERAL ERROR	
	MM	INCHES	MM	INCHES
A_2	0.020	0.0008	>0.250	>0.0100
B_1	>0.250	>0.0100	0.0151	0.0006
B_2	>0.250	>0.0100	0.025	0.0010
R_1	0.040	.0016	>0.250	>0.0100
R_2	0.100	.0040	>0.0250	>0.0100

4.0 DETECTOR OPTICAL SYSTEM

4.1 Optical Arrangement and Function of Detector Optics

Each of the TOVS-BSU double-sphere Cassegrainian telescopes, whether it be an 80- or 61-mm OD telescope, is followed by two separate detector channels, optically split by a dichroic filter beamsplitter, as illustrated in Figure 4-1. The beamsplitter is mounted at 45 degrees to the telescope optical axis so that the axis of the reflective channel is at 90 degrees to the transmittive channel which remains parallel to the telescope optical axis. All fourteen detector channels, whether in the reflective or transmissive location have the same functional elements from the dichroic filter to the detector, namely, two bandpass filters for spectral bandpass selection, a doublet lens for imaging the telescope secondary mirror on the detector surface, and a window to seal the detector and its surroundings. Both because of the large spectral range covered by different channels, and because two different-sized telescopes are used, two different lens materials are used and three different doublet lens designs are required.

4.2 Design of Detector Optics for Each of the Fourteen Channels

Doublet lenses have been used in each of the fourteen channels because a singlet lens cannot produce an image of the secondary mirror of good-enough quality on the detector. The ray-trace axis systems which were used for designing and analyzing the doublet lens used in each of the fourteen channels is shown in Figure 4-2. Figure 4-2 is an accurate computer plot of selected rays including the boundary rays for both channel 11, a reflective channel, and channel 8, a transmissive channel. Table 4-1 describes the ray-trace axis systems to be used for all other reflective channels, and Tables 4-2 through 4-8 give the dimensional parameters used for the ray traces of reflective channels 1, 2, 3, 4, 11, 12, and 13, respectively.

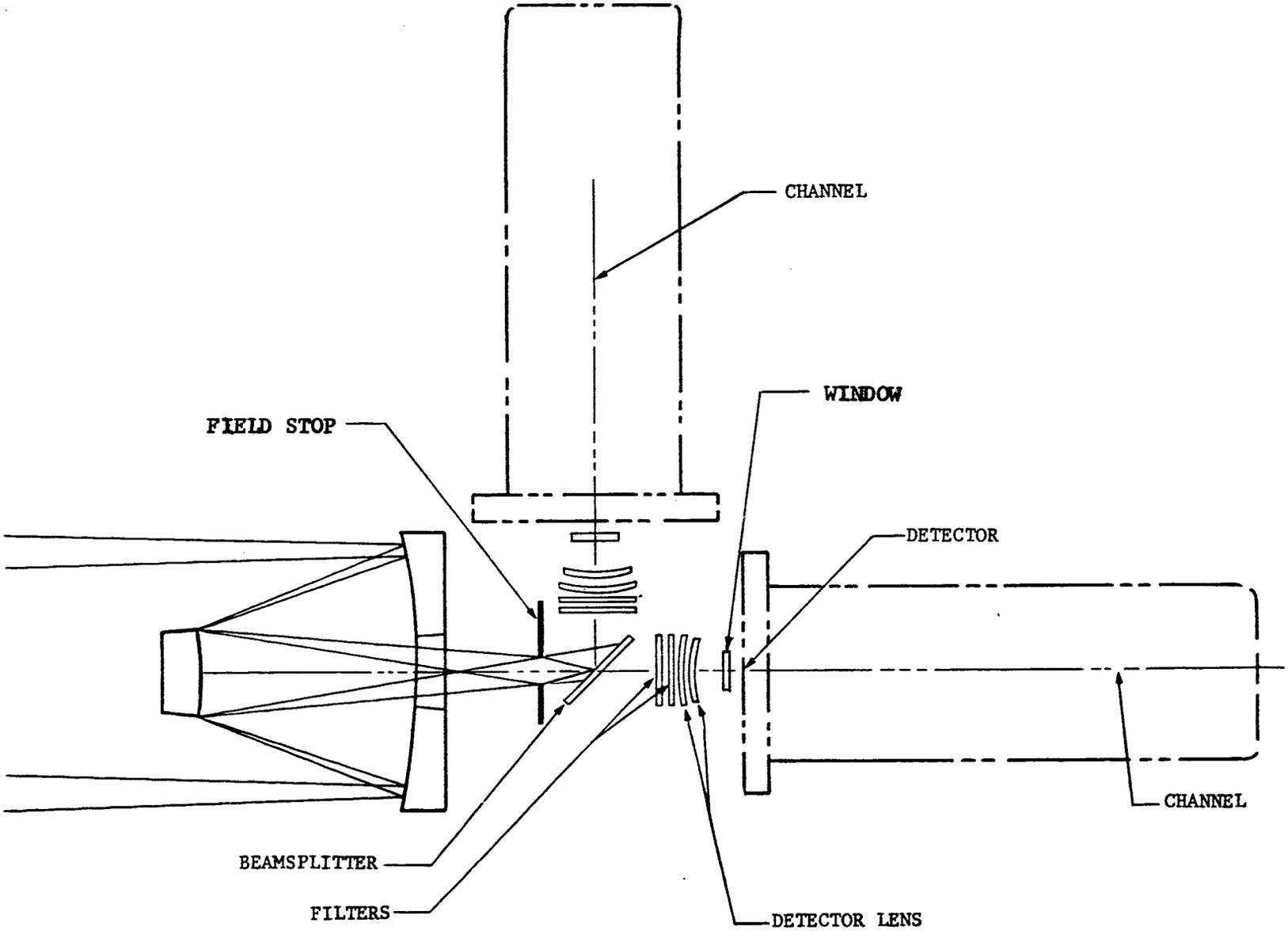

Figure 4-1. Optical Schematic Showing Two Detector Optical Channels Following Each Telescope

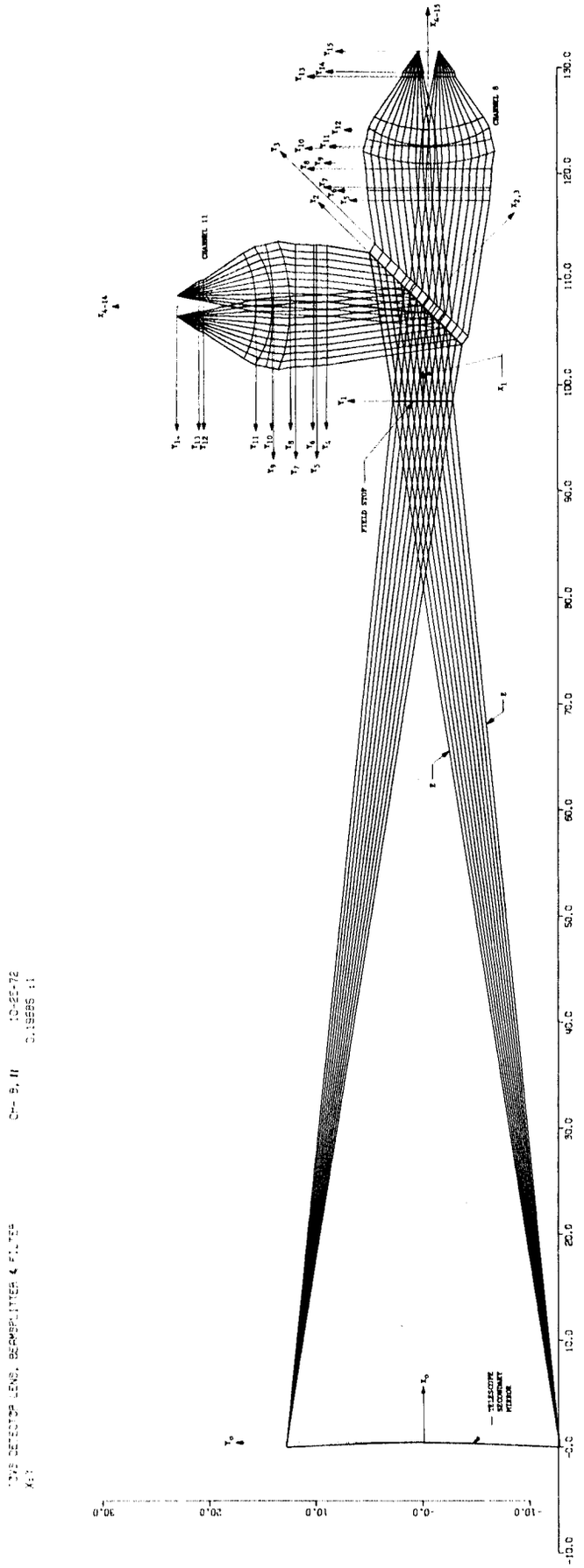

Figure 4-2. Ray-Trace Axis Systems for Reflected Channel 11 and Transmitted Channel 8

TABLE 4-1 (SHEET 1 OF 3). DESCRIPTION OF THE RAY-TRACE AXIS SYSTEMS USED FOR ALL REFLECTIVE DETECTOR CHANNELS

The ray-trace starting points are located on the telescope secondary mirror, and rays are traced successively to the field stop, dichroic filter beamsplitter, spectral bandpass filters, detector doublet lens and the detector sensitive area.

(X_o,Y_o,Z_o)	Telescope Secondary Mirror--The apex of the secondary mirror surface is located at the origin of the (X_o, Y_o,Z_o) axis system. However, the secondary mirror is not active in this ray trace. It is used only as the starting surface for this ray trace, since it is imaged on the detector.
(X_1,Y_1,Z_1)	Field Stop--The field stop lies in the Y_1-Z_1 plane, and performs the function of aperture stop for the detector optical system. Thus each family of rays starting from a point on the telescope secondary mirror must intersect the circular area of the field stop in precisely the same uniform area array of points.
(X_2,Y_2,Z_2)	First Surface of Dichroic Filter Beamsplitter--This is a reflecting plane surface in the Y_2-Z_2 plane which is rotated 45° about the Z_1-axis from the Y_1-Z_1 plane.
(X_3,Y_3,Z_3)	Mathematical Axis System--This axis system facilitates locating the (X_4,Y_4,Z_4) axis system.
(X_4,Y_4,Z_4)	First Surface of First Filter--This is a refracting plane surface in the Y_4-Z_4 plane.
(X_5,Y_5,Z_5)	Second Surface of First Filter--This is a refracting plane surface in the Y_5-Z_5 plane.

TABLE 4-1 (SHEET 2 OF 3) DESCRIPTION OF THE RAY-TRACE AXIS SYSTEMS USED FOR ALL REFLECTIVE DETECTOR CHANNELS

(X_6,Y_6,Z_6)	First Surface of Second Filter--This is a refracting plane surface in the Y_6-Z_6 plane.
(X_7,Y_7,Z_7)	Second Surface of Second Filter--This is a refracting plane surface in the Y_7-Z_7 plane.
(X_8,Y_8,Z_8)	First Surface of First Lens--This is a refracting spherical surface with its apex at the origin of the (X_8,Y_8,Z_8) axis system and its center on the positive X_8-axis.
(X_9,Y_9,Z_9)	Second Surface of First Lens--This is a refracting spherical surface with its apex at the origin of the (X_9,Y_9,Z_9) axis system and its center on the positive X_9-axis.
(X_{10},Y_{10},Z_{10})	First Surface of Second Lens--This is a refracting spherical surface with its apex at the orign of the (X_{10},Y_{10},Z_{10}) axis system and its center on the positive X_{10}-axis.
(X_{11},Y_{11},Z_{11})	Second Surface of Second Lens--This is a refracting spherical surface with its apex at the origin of the (X_{11},Y_{11},Z_{11}) axis system and its center on the positive X_{11}-axis.
(X_{12},Y_{12},Z_{12})	First Surface of Detector Window--This is a refracting plane surface in the Y_{12}-Z_{12} plane.
(X_{13},Y_{13},Z_{13})	Second Surface of Detector Window--This is a refracting plane surface in the Y_{13}-Z_{13} plane.

TABLE 4-1 (SHEET 3 OF 3). DESCRIPTION OF THE RAY-TRACE AXIS SYSTEMS USED FOR ALL REFLECTIVE DETECTOR CHANNELS

(X_{14}, Y_{14}, Z_{14})	Detector Surface--This is a plane surface in the Y_{14}-Z_{14} plane. It is used to measure ray locations at the detector sensitive surface.

TABLE 4-2 (SHEET 1 OF 3). DIMENSIONAL PARAMETERS FOR CHANNEL 1 (REFLECTIVE)

Axis Sub-Script (n)	Optical Function of Surface	A_n (mm)	B_n (mm)	C_n (mm)	α_n (deg)	β_n (deg)	γ_n (deg)	Surface Shape	D_n (mm)	E_n (mm)	F_n (mm)	R_n (mm)	N_n (mm)
1	FOV Stop	74.860						Plane					1.0000
2	Dichroic Reflec-tion	9.000				-45.0		Plane					1.0000
3	Mathemat-ical aid					135.0		Plane					1.0000
4	First Sur. First Filter	9.000						Plane					4.0270
5	Second Sur. First Filter	1.000						Plane					1.0000
6	First Sur. Second Filter	0.250						Plane					1.6875

TABLE 4-2 (SHEET 2 OF 3). DIMENTIONAL PARAMETERS FOR CHANNEL 1 (REFLECTIVE)

Axis Sub-Script (n)	Optical Function of Surface	A_n (mm)	B_n (mm)	C_n (mm)	α_n (deg)	β_n (deg)	γ_n (deg)	Surface Shape	D_n (mm)	E_n (mm)	F_n (mm)	R_n (mm)	N_n (mm)
7	Second Sur. Second Filter	1.000						Plane					1.0000
8	First Sur. First Lens	1.250						Sphere	1.0	1.0	1.0	18.476	4.0270
9	Second Sur. First Lens	1.550						Sphere	1.0	1.0	1.0	30.570	1.0000
10	First Sur. Second Lens	0.100						Sphere	1.0	1.0	1.0	9.055	4.0270
11	Second Sur. Second Lens	1.550						Sphere	1.0	1.0	1.0	9.843	1.0000
12	First Sur. Window	5.000						Plane					4.0270

TABLE 4-2 (SHEET 3 OF 3). DIMENSIONAL PARAMETERS FOR CHANNEL 1 (REFLECTIVE)

Axis Sub-Script (n)	Optical Function of Surface	A_n (mm)	B_n (mm)	C_n (mm)	α_n (deg)	β_n (deg)	γ_n (deg)	Surface Shape	D_n (mm)	E_n (mm)	F_n (mm)	R_n (mm)	N_n (mm)
13	Second Sur. Window	0.380						Plane					1.0000
14	Detector Surface	1.014						Plane					1.0000

TABLE 4-3 (SHEET 1 OF 3). DIMENSIONAL PARAMETERS FOR CHANNEL 2 (REFLECTIVE)

Axis Sub-Script (n)	Optical Function of Surface	A_n (mm)	B_n (mm)	C_n (mm)	α_n (deg)	β_n (deg)	γ_n (deg)	Surface Shape	D_n (mm)	E_n (mm)	F_n (mm)	R_n (mm)	N_n (mm)
1	FOV Stop	98.440						Plane					1.0000
2	Dichroic Reflec-tion	9.000				-45.0		Plane					1.0000
3	Mathemat-ical aid					135.0		Plane					1.0000
4	First Sur. First Filter	9.000						Plane					4.0220
5	Second Sur. First Filter	1.000						Plane					1.0000
6	First Sur. Second Filter	0.250						Plane					1.6637

TABLE 4-3 (SHEET 2 OF 3). DIMENSIONAL PARAMETERS FOR CHANNEL 2 (REFLECTIVE)

Axis Sub-Script (n)	Optical Function of Surface	A_n (mm)	B_n (mm)	C_n (mm)	α_n (deg)	β_n (deg)	γ_n (deg)	Surface Shape	D_n (mm)	E_n (mm)	F_n (mm)	R_n (mm)	N_n (mm)
7	Second Sur. Second Filter	1.000						Plane					1.0000
8	First Sur. First Lens	1.250						Sphere	1.0	1.0	1.0	17.456	4.0220
9	Second Sur. First Lens	1.550						Sphere	1.0	1.0	1.0	23.685	1.0000
10	First Sur. Second Lens	0.100						Sphere	1.0	1.0	1.0	10.128	4.0220
11	Second Sur. Second Lens	1.550						Sphere	1.0	1.0	1.0	11.567	1.0000

TABLE 4-3 (SHEET 3 OF 3). DIMENSIONAL PARAMETERS FOR CHANNEL 2 (REFLECTIVE)

Axis Sub-Script (n)	Optical Function of Surface	A_n (mm)	B_n (mm)	C_n (mm)	α_n (deg)	β_n (deg)	γ_n (deg)	Surface Shape	D_n (mm)	E_n (mm)	F_n (mm)	R_n (mm)	N_n (mm)
12	First Sur. Window	5.000						Plane					4.0220
13	Second Sur. Window	0.380						Plane					1.0000
14	Detector Surface	2.003						Plane					1.0000

TABLE 4-4 (SHEET 1 OF 3). DIMENSIONAL PARAMETERS FOR CHANNEL 3 (REFLECTIVE)

Axis Sub-Script (n)	Optical Function of Surface	A_n (mm)	B_n (mm)	C_n (mm)	n (deg)	n (deg)	n (deg)	Surface Shape	D_n (mm)	E_n (mm)	F_n (mm)	R_n (mm)	N_n (mm)
1	FOV Stop	74.860						Plane					1.0000
2	Dichroic Reflec-tion	9.000				-45.0		Plane					1.0000
3	Mathemat-ical aid					135.0		Plane					1.0000
4	First Sur. First Filter	9.000						Plane					4.0032
5	Second Sur. First Filter	1.000						Plane					1.0000
6	First Sur. Second Filter	0.250						Plane					2.2023

TABLE 4-4 (SHEET 2 OF 3). DIMENSIONAL PARAMETERS FOR CHANNEL 3 (REFLECTIVE)

Axis Sub-Script (n)	Optical Function of Surface	A_n (mm)	B_n (mm)	C_n (mm)	α_n (deg)	β_n (deg)	γ_n (deg)	Surface Shape	D_n (mm)	E_n (mm)	F_n (mm)	R_n (mm)	N_n (mm)
7	Second Sur. Second Filter	1.000						Plane					1.0000
8	First Sur. First Lens	1.250						Sphere	1.0	1.0	1.0	18.476	4.0032
9	Second Sur. First Lens	1.550						Sphere	1.0	1.0	1.0	30.570	1.0000
10	First Sur. Second Lens	0.100						Sphere	1.0	1.0	1.0	9.055	4.0032
11	Second Sur. Second Lens	1.550						Sphere	1.0	1.0	1.0	9.843	1.0000

TABLE 4-4 (SHEET 3 OF 3). DIMENSIONAL PARAMETERS FOR CHANNEL 3 (REFLECTIVE)

Axis Sub-Script (n)	Optical Function of Surface	A_n (mm)	B_n (mm)	C_n (mm)	α_n (deg)	β_n (deg)	γ_n (deg)	Surface Shape	D_n (mm)	E_n (mm)	F_n (mm)	R_n (mm)	N_n (mm)
12	First Sur. Window	5,000						Plane					4.0032
13	Second Sur. Window	0.380						Plane					1.0000
14	Detector Surface	1.078						Plane					1.0000

TABLE 4-5 (SHEET 1 OF 3). DIMENSIONAL PARAMETERS FOR CHANNEL 4 (REFLECTIVE)

Axis Sub-Script (n)	Optical Function of Surface	A_n (mm)	B_n (mm)	C_n (mm)	α_n (deg)	β_n (deg)	γ_n (deg)	Surface Shape	D_n (mm)	E_n (mm)	F_n (mm)	R_n (mm)	N_n (mm)
1	FOV Stop	74.860						Plane					1.0000
2	Dichroic Reflec-tion	9.000				-45.0		Plane					1.0000
3	Mathemat-ical Aid					135.0		Plane					1.0000
4	First Sur. First Filter	9.000						Plane					4.0026
5	Second Sur. First Filter	1.000						Plane					1.0000
6	First Sur. Second Filter	0.250						Plane					2.1825

TABLE 4-5 (SHEET 2 OF 3). DIMENSIONAL PARAMETERS FOR CHANNEL 4 (REFLECTIVE)

Axis Sub-Script (n)	Optical Function of Surface	A_n (mm)	B_n (mm)	C_n (mm)	α_n (deg)	β_n (deg)	γ_n (deg)	Surface Shape	D_n (mm)	E_n (mm)	F_n (mm)	R_n (mm)	N_n (mm)
7	Second Sur. Second Filter	1.000						Plane					1.0000
8	First Sub. First Lens	1.250						Sphere	1.0	1.0	1.0	18.476	4.0026
9	Second Sur. First Lens	1.550						Sphere	1.0	1.0	1.0	30.570	1.0000
10	First Sur. Second Lens	0.100						Sphere	1.0	1.0	1.0	9.055	4.0026
11	Second Sur. Second Lens	1.550						Sphere	1.0	1.0	1.0	9.843	1.0000

TABLE 4-5 (SHEET 3 OF 3). DIMENSIONAL PARAMETERS FOR CHANNEL 4 (REFLECTIVE)

Axis Sub-Script (n)	Optical Function of Surface	A_n (mm)	B_n (mm)	C_n (mm)	α_n (deg)	β_n (deg)	γ_n (deg)	Surface Shape	D_n (mm)	E_n (mm)	F_n (mm)	R_n (mm)	N_n (mm)
12	First Sur. Window	5.000						Plane					4.0260
13	Second Sur. Window	0.380						Plane					1.0000
14	Detector Surface	1.079						Plane					1.0000

TABLE 4-6 (SHEET 1 OF 3). DIMENSIONAL PARAMETERS FOR CHANNEL 11 (REFLECTIVE)

Axis Sub-Script (n)	Optical Function of Surface	A_n (mm)	B_n (mm)	C_n (mm)	α_n (deg)	β_n (deg)	γ_n (deg)	Surface Shape	D_n (mm)	E_n (mm)	F_n (mm)	R_n (mm)	N_n (mm)
1	FOV Stop	98.440						Plane					1.0000
2	Dichroic Reflec-tion	9.000				-45.0		Plane					1.0000
3	Mathemat-ical Aid					135.0		Plane					1.0000
4	First Sur. First Filter	9.000						Plane					4.0016
5	Second Sur. First Filter	1.000						Plane					1.0000
6	First Sur. Second Filter	0.250						Plane					2.3703

TABLE 4-6 (SHEET 2 OF 3). DIMENSIONAL PARAMETERS FOR CHANNEL 11 (REFLECTIVE)

Axis Sub-Script (n)	Optical Function of Surface	A_n (mm)	B_n (mm)	C_n (mm)	α_n (deg)	β_n (deg)	γ_n (deg)	Surface Shape	D_n (mm)	E_n (mm)	F_n (mm)	R_n (mm)	N_n (mm)
7	Second Sur. Second Filter	1.750						Plane					1.0000
8	First Sur. First Lens	0.500						Sphere	1.0	1.0	1.0	17.456	4.0016
9	Second Sur. First Lens	1.550						Sphere	1.0	1.0	1.0	23.685	1.0000
10	First Sur. Second Lens	0.100						Sphere	1.0	1.0	1.0	10.128	4.0016
11	Second Sur. Second Lens	1.550						Sphere	1.0	1.0	1.0	11.567	1.0000
12	First Sur. Window	5.000						Plane					4.0016

TABLE 4-6 (SHEET 3 OF 3). DIMENSIONAL PARAMETERS FOR CHANNEL 11 (REFLECTIVE)

Axis Sub-Script (n)	Optical Function of Surface	A_n (mm)	B_n (mm)	C_n (mm)	α_n (deg)	β_n (deg)	γ_n (deg)	Surface Shape	D_n (mm)	E_n (mm)	F_n (mm)	R_n (mm)	N_n (mm)
13	Second Sur. Window	0.380						Plane					1.0000
14	Detector Surface	2.065						Plane					1.0000

TABLE 4-7 (SHEET 1 OF 3). DIMENSIONAL PARAMETERS FOR CHANNEL 12 (REFLECTIVE)

Axis Sub-Script (n)	Optical Function of Surface	A_n (mm)	B_n (mm)	C_n (mm)	α_n (deg)	β_n (deg)	γ_n (deg)	Surface Shape	D_n (mm)	E_n (mm)	F_n (mm)	R_n (mm)	N_n (mm)
1	FOV Stop	98.440						Plane					1.0000
2	Dichroic Reflec-tion	9.000			-45.0			Plane					1.0000
3	Mathemat-ical Aid				135.0			Plane					1.0000
4	First Sur. First Filter	9.000						Plane					3.4140
5	Second Sur. First Filter	1.000						Plane					1.0000
6	First Sur. Second Filter	0.250						Plane					2.6470

TABLE 4-7 (SHEET 2 OF 3). DIMENSIONAL PARAMETERS FOR CHANNEL 12 (REFLECTIVE)

Axis Sub-Script (n)	Optical Function of Surface	A_n (mm)	B_n (mm)	C_n (mm)	α_n (deg)	β_n (deg)	γ_n (deg)	Surface Shape	D_n (mm)	E_n (mm)	F_n (mm)	R_n (mm)	N_n (mm)
7	Second Sur. Second Filter	1.750						Plane					1.0000
8	First Sur. First Lens	0.500						Sphere	1.0	1.0	1.0	15.677	3.4140
9	Second Sur. First Lens	1.550						Sphere	1.0	1.0	1.0	21.325	1.0000
10	First Sur. Second Lens	0.100						Sphere	1.0	1.0	1.0	8.921	3.4140
11	Second Sur. Second Lens	1.550						Sphere	1.0	1.0	1.0	10.500	1.0000

TABLE 4-7 (SHEET 3 OF 3). DIMENSIONAL PARAMETERS FOR CHANNEL 12 (REFLECTIVE)

Axis Sub-Script (n)	Optical Function of Surface	A_n (mm)	B_n (mm)	C_n (mm)	α_n (deg)	β_n (deg)	γ_n (deg)	Surface Shape	D_n (mm)	E_n (mm)	F_n (mm)	R_n (mm)	N_n (mm)
12	First Sur. Window	5.000						Plane					3.4140
13	Second Sur. Window	0.380						Plane					1.0000
14	Detector Surface	2.097						Plane					1.0000

TABLE 4-8 (SHEET 1 OF 3). DIMENSIONAL PARAMETERS FOR CHANNEL 13 (REFLECTIVE)

Axis Sub-Script (n)	Optical Function of Surface	A_n (mm)	B_n (mm)	C_n (mm)	α_n (deg)	β_n (deg)	γ_n (deg)	Surface Shape	D_n (mm)	E_n (mm)	F_n (mm)	R_n (mm)	N_n (mm)
1	FOV Stop	98.440						Plane					1.0000
2	Dichroic Reflec-tion	9.000				-45.0		Plane					1.0000
3	Mathemat-ical Aid					135.0		Plane					1.0000
4	First Sur. First Filter	9.000						Plane					3.4124
5	Second Sur. First Filter	1.000						Plane					1.0000
6	First Sur. Second Filter	0.250						Plane					2.6360
7	Second Sur. Second Filter	1.750						Plane					1.0000

TABLE 4-8 (SHEET 2 OF 3). DIMENSIONAL PARAMETERS FOR CHANNEL 13 (REFLECTIVE)

Axis Sub-Script (n)	Optical Function of Surface	A_n (mm)	B_n (mm)	C_n (mm)	α_n (deg)	β_n (deg)	γ_n (deg)	Surface Shape	D_n (mm)	E_n (mm)	F_n (mm)	R_n (mm)	N_n (mm)
8	First Sur. First Lens	0.500						Sphere	1.0	1.0	1.0	15.677	3.4124
9	Second Sur. First Lens	1.550						Sphere	1.0	1.0	1.0	21.325	1.0000
10	First Sur. Second Lens	0.100						Sphere	1.0	1.0	1.0	8.912	3.4124
11	Second Sur. Second Lens	1.550						Sphere	1.0	1.0	1.0	10.500	1.0000
12	First Sur. Window	5.000						Plane					3.4124

TABLE 4-8 (SHEET 3 OF 3). DIMENSIONAL PARAMETERS FOR CHANNEL 13 (REFLECTIVE)

Axis Sub-Script (n)	Optical Function of Surface	A_n (mm)	B_n (mm)	C_n (mm)	α_n (deg)	β_n (deg)	γ_n (deg)	Surface Shape	D_n (mm)	E_n (mm)	F_n (mm)	R_n (mm)	N_n (mm)
13	Second Sur. Window	0.380						Plane					1.0000
14	Detector Surface	2.103						Plane					1.0000

Table 4-9 describes the ray-trace axis system to be used with all transmissive channels, and Tables 4-10 through 4-16 give the dimensional parameters used for the ray-trace transmissive channels 5, 6, 7, 8, 9, 10, and 14, respectively.

4.3 Design and Performance of the Detector Doublet Lenses

The fourteen detector channels require three different lens designs for the detector doublet. Channels 1, 3, 4, 5, 6, and 7 use two germanium elements with their radii optimized for the 61-mm OD telescope. Channels 2, 8, 9, 10, and 11 also use two germanium elements, but with radii optimized for the 80-mm OD telescope. Finally, channels 12, 13, and 14 use two silicon elements which are optimized for the 80-mm OD telescope.

Table 4-17 summarizes pertinent design features for each of the fourteen detector channels. The last seven columns of Table 4-17 list the resultant image characteristics at the detector for ray-traces using 200-ray families from starting points at the top and bottom edges of the telescope secondary mirror. These two starting points are on the $+Y_o$-axis and $-Y_o$-axis, respectively, in Figure 4-2, so $Z_o = 0$. Each 200-ray family was required to fill the circular field stop in the same uniform area array. Thus, the field stop is the aperture stop of the detector optics. The image of the starting point for each 200-ray family from the edge of the telescope secondary mirror is focused on the detector surface. To produce each 200-ray image at the detector surface, the computer automatically modified the detector axial location: A_{14} for reflective channels, and A_{15} for transmissive channels until the 200-ray image had a minimum least square spread measured radially to the sensitive diameter of the detector, or along the Y_{14} or Y_{15} coordinator of the detector in the reflective and transmissive channels, respectively.

The back focal distance listed in Table 4-17 is to total focused distance from the last surface of the doublet lens to the detector surface. This includes the window in this distance. The centroid Y value in Table 4-17 is the half-power radius of the detector which just matches the telescope secondary mirror image. Centroid Z is zero in all cases.

TABLE 4-9 (SHEET 1 OF 3). DESCRIPTION OF THE RAY-TRACE AXIS SYSTEMS USED FOR ALL TRANSMISSIVE DETECTOR CHANNELS

The ray trace starting points are located on the telescope secondary mirror, and rays are traced successively to the field stop, dichroic filter beamsplitter, spectral bandpass filters, detector doublet lens and the detector sensitive area.

(X_o,Y_o,Z_o)	Telescope Secondary Mirror--The apex of the secondary mirror surface is located at the origin of the (X_o,Y_o,Z_o) axis system. However, the secondary mirror is not active in this ray trace. It is used only as the starting surface for this ray trace, since it is imaged on the detector.
(X_1,Y_1,Z_1)	Field Stop--The field stop lies in the Y_1-Z_1 plane, and performs the function of aperture stop for the detector optical system. Thus each family of rays starting from a point on the telescope secondary mirror must intersect the circular area of the field stop in precisely the same uniform area array of points.
(X_2,Y_2,Z_2)	First Surface of Dichroic Filter Beamsplitter--This is a refracting plane surface in the Y_2-Z_2 plane which is rotated 45° about the Z_1-axis from the Y_1-Z_1 plane.
(X_3,Y_3,Z_3)	Second Surface of Dichroic Filter Beamsplitter--This is a refracting plane surface in the Y_3-Z_3 plane.
(X_4,Y_4,Z_4)	Mathematical Axis System--This axis system facilitates in locating the (X_5,Y_5,Z_5) Axis System.
(X_5,Y_5,Z_5)	First Surface of First Filter--This is a refracting plane surface in the Y_5-Z_5 plane.

TABLE 4-9 (SHEET 2 OF 3). DESCRIPTION OF THE RAY-TRACE AXIS SYSTEMS USED FOR ALL TRANSMISSIVE DETECTOR CHANNELS

(X_6,Y_6,Z_6)	Second Surface of First Filter--This is a refracting plane surface in the Y_6-Z_6 plane.
(X_7,Y_7,Z_7)	First Surface of Second Filter--This is a refracting plane surface in the Y_7-Z_7 plane.
(X_8,Y_8,Z_8)	Second Surface of Second Filter--This is a refracting plane surface in the Y_8-Z_8 plane.
(X_9,Y_9,Z_9)	First Surface of First Lens--This is a refracting spherical surface with its apex at the origin of the (X_9,Y_9,Z_9) axis system and its center on the positive X_9-axis.
(X_{10},Y_{10},Z_{10})	Second Surface of First Lens--This is a refracting spherical Surface with its apex at the origin of the (X_{10},Y_{10},Z_{10}) axis system and its center on the positive X_{10}-axis.
(X_{11},Y_{11},Z_{11})	First Surface of Second Lens--This is a refracting spherical surface with its apex at the origin of the (X_{11},Y_{11},Z_{11}) axis system and its center on the positive X_{11}-axis.
(X_{12},Y_{12},Z_{12})	Second Surface of Second Lens--This is a refracting spherical surface with its apex at the origin of the (X_{12},Y_{12},Z_{12}) axis system and its center on the positive X_{12}-axis.
(X_{13},Y_{13},Z_{13})	First Surface of Detector Window--This is a refracting plane surface in the Y_{13}-Z_{13} plane.

TABLE 4-9 (SHEET 3 OF 3). DESCRIPTION OF THE RAY-TRACE AXIS SYSTEMS USED FOR ALL TRANSMISSIVE DETECTOR CHANNELS

(X_{14},Y_{14},Z_{14})	Second Surface of Detector Window--This is a refracting plane surface in the Y_{14}-Z_{14} plane.
(X_{15},Y_{15},Z_{15})	Detector Surface--This is a plane surface in the Y_{15}-Z_{15} plane. It is used to measure ray locations at the detector sensitive surface.

TABLE 4-10 (SHEET 1 OF 3). DIMENSIONAL PARAMETERS FOR CHANNEL 5 (TRANSMISSIVE)

Axis Sub-Script (n)	Optical Function of Surface	A_n (mm)	B_n (mm)	C_n (mm)	α_n (deg)	β_n (deg)	γ_n (deg)	Surface Shape	D_n (mm)	E_n (mm)	F_n (mm)	R_n (mm)	N_n (mm)
1	FOV Stop	74.860						Plane					1.0000
2	First Sur. Dichroic	9.000				-45.0		Plane					4.0018
3	Second Sur. Dichroic	1.000						Plane					1.0000
4	Mathematical Aid	-1.000				45.0		Plane					1.0000
5	First Sur. First Filter	10.000	-0.58					Plane					4.0018
6	Second Sur. First Filter	1.000						Plane					1.0000
7	First Sur. Second Filter	0.250						Plane					2.3832

TABLE 4-10 (SHEET 2 OF 3). DIMENSIONAL PARAMETERS FOR CHANNEL 5 (TRANSMISSIVE)

Axis Sub-Script (n)	Optical Function of Surface	A_n (mm)	B_n (mm)	C_n (mm)	α_n (deg)	β_n (deg)	γ_n (deg)	Surface Shape	D_n (mm)	E_n (mm)	F_n (mm)	R_n (mm)	N_n (mm)
8	Second Sur. Second Filter	1.750						Plane					1.0000
9	First Sur. First Lens	0.500						Sphere	1.0	1.0	1.0	18.476	4.0018
10	Second Sur. First Lens	1.550						Sphere	1.0	1.0	1.0	30.570	1.0000
11	First Sur. Second Lens	0.100						Sphere	1.0	1.0	1.0	9.055	4.0018
12	Second Sur. Second Lens	1.550						Sphere	1.0	1.0	1.0	9.843	1.0000

TABLE 4-10 (SHEET 3 OF 3). DIMENSIONAL PARAMETERS FOR CHANNEL 5 (TRANSMISSIVE)

Axis Sub-Script (n)	Optical Function of Surface	A_n (mm)	B_n (mm)	C_n (mm)	α_n (deg)	β_n (deg)	γ_n (deg)	Surface Shape	D_n (mm)	E_n (mm)	F_n (mm)	R_n (mm)	N_n (mm)
13	First Sur. Window	5.000						Plane					4.0018
14	Second Sur. Window	0.380						Plane					1.0000
15	Detector Surface	1.083						Plane					1.0000

TABLE 4-11 (SHEET 1 OF 3). DIMENSIONAL PARAMETERS FOR CHANNEL 6 (TRANSMISSIVE)

Axis Sub-Script (n)	Optical Function of Surface	A_n (mm)	B_n (mm)	C_n (mm)	α_n (deg)	β_n (deg)	γ_n (deg)	Surface Shape	D_n (mm)	E_n (mm)	F_n (mm)	R_n (mm)	N_n (mm)
1	FOV Stop	74.860						Plane					1.0000
2	First Sur. Dichroic	9.000				-45.0		Plane					4.0018
3	Second Sur. Dichroic	1.000						Plane					1.0000
4	Mathematical Aid	-1.000				45.0		Plane					1.0000
5	First Sur. First Filter	10.000	-0.58					Plane					4.0018
6	Second Sur. First Filter	1.000						Plane					1.0000

TABLE 4-11 (SHEET 2 OF 3). DIMENSIONAL PARAMETERS FOR CHANNEL 6 (TRANSMISSIVE)

Axis Sub-Script (n)	Optical Function of Surface	A_n (mm)	B_n (mm)	C_n (mm)	α_n (deg)	β_n (deg)	γ_n (deg)	Surface Shape	D_n (mm)	E_n (mm)	F_n (mm)	R_n (mm)	N_n (mm)
7	First Sur. Second Filter	0.250						Plane					2.3815
8	Second Sur. Second Filter	1.750						Plane					1.0000
9	First Sur. First Lens	0.500						Sphere	1.0	1.0	1.0	18.476	4.0018
10	Second Sur. First Lens	1.550						Sphere	1.0	1.0	1.0	30.570	1.0000
11	First Sur. Second Lens	0.100						Sphere	1.0	1.0	1.0	9.055	4.0018

TABLE 4-11 (SHEET 3 OF 3). DIMENSIONAL PARAMETERS FOR CHANNEL 6 (TRANSMISSIVE)

Axis Sub-Script (n)	Optical Function of Surface	A_n (mm)	B_n (mm)	C_n (mm)	α_n (deg)	β_n (deg)	γ_n (deg)	Surface Shape	D_n (mm)	E_n (mm)	F_n (mm)	R_n (mm)	N_n (mm)
12	Second Sur. Second Lens	1.550						Sphere	1.0	1.0	1.0	9.843	1.0000
13	First Sur. Window	5.000						Plane					4.0018
14	Second Sur. Window	0.380						Plane					1.0000
15	Detector Surface	1.083						Plane					1.0000

TABLE 4-12 (SHEET 1 OF 3). DIMENSIONAL PARAMETERS FOR CHANNEL 7 (TRANSMISSIVE)

Axis Sub-Script (n)	Optical Function of Surface	A_n (mm)	B_n (mm)	C_n (mm)	α_n (deg)	β_n (deg)	γ_n (deg)	Surface Shape	D_n (mm)	E_n (mm)	F_n (mm)	R_n (mm)	N_n (mm)
1	FOV Stop	74.860						Plane					1.0000
2	First Sur. Dichroic	9.000				-45.0		Plane					4.0017
3	Second Sur. Dichroic	1.000						Plane					1.0000
4	Mathemat-ical Aid	-1.000				45.0		Plane					1.0000
5	First Sur. First Filter	10.000	-0.58					Plane					4.0017
6	Second Sur. First Filter	1.000						Plane					1.0000

TABLE 4-12 (SHEET 2 OF 3). DIMENSIONAL PARAMETERS FOR CHANNEL 7 (TRANSMISSIVE)

Axis Sub-Script (n)	Optical Function of Surface	A_n (mm)	B_n (mm)	C_n (mm)	α_n (deg)	β_n (deg)	γ_n (deg)	Surface Shape	D_n (mm)	E_n (mm)	F_n (mm)	R_n (mm)	N_n (mm)
7	First Sur. Second Filter	0.250						Plane					2.3780
8	Second Sur. Second Filter	1.750						Plane					1.0000
9	First Sur. First Lens	0.500						Sphere	1.0	1.0	1.0	18.476	4.0017
10	Second Sur. First Lens	1.550						Sphere	1.0	1.0	1.0	30.570	1.0000
11	First Sur. Second Lens	0.100						Sphere	1.0	1.0	1.0	9.055	4.0017

TABLE 4-12 (SHEET 2 OF 3). DIMENSIONAL PARAMETERS FOR CHANNEL 7 (TRANSMISSIVE)

Axis Sub-Script (n)	Optical Function of Surface	A_n (mm)	B_n (mm)	C_n (mm)	α_n (deg)	β_n (deg)	γ_n (deg)	Surface Shape	D_n (mm)	E_n (mm)	F_n (mm)	R_n (mm)	N_n (mm)
12	Second Sur. Second Lens	1.550						Sphere	1.0	1.0	1.0	9.843	1.0000
13	First Sur. Window	5.000						Plane					4.0017
14	Second Sur. Window	0.380						Plane					1.0000
15	Detector Surface	1.083						Plane					1.0000

TABLE 4-13 (SHEET 1 OF 3). DIMENSIONAL PARAMETERS FOR CHANNEL 8 (TRANSMISSIVE)

Axis Sub-Script (n)	Optical Function of Surface	A_n (mm)	B_n (mm)	C_n (mm)	α_n (deg)	β_n (deg)	γ_n (deg)	Surface Shape	D_n (mm)	E_n (mm)	F_n (mm)	R_n (mm)	N_n (mm)
1	FOV Stop	98.440						Plane					1.0000
2	First Sur. Dichroic	9.000				-45.0		Plane					4.0017
3	Second Sur. Dichroic	1.000						Plane					1.0000
4	Mathematical Aid	-1.000				45.0		Plane					1.0000
5	First Sur. First Filter	10.000	-.58					Plane					4.0017
6	Second Sur. First Filter	1.000						Plane					1.0000
7	First Sur. Second Filter	0.250						Plane					2.3756

TABLE 4-13 (SHEET 2 OF 3). DIMENSIONAL PARAMETERS FOR CHANNEL 8 (TRANSMISSIVE)

Axis Sub-Script (n)	Optical Function of Surface	A_n (mm)	B_n (mm)	C_n (mm)	α_n (deg)	β_n (deg)	γ_n (deg)	Surface Shape	D_n (mm)	E_n (mm)	F_n (mm)	R_n (mm)	N_n (mm)
8	Second Sur. Second Filter	1.750						Plane					1.0000
9	First Sur. First Lens	0.500						Sphere	1.0	1.0	1.0	17.456	4.0017
10	Second Sur. First Lens	1.550						Sphere	1.0	1.0	1.0	23.685	1.0000
11	First Sur. Second Lens	0.100						Sphere	1.0	1.0	1.0	10.128	4.0017
12	Second Sur. Second Lens	1.550						Sphere	1.0	1.0	1.0	11.567	1.0000

TABLE 4-13 (SHEET 3 OF 3). DIMENSIONAL PARAMETERS FOR CHANNEL 8 (TRANSMISSIVE)

Axis Sub-Script (n)	Optical Function of Surface	A_n (mm)	B_n (mm)	C_n (mm)	α_n (deg)	β_n (deg)	γ_n (deg)	Surface Shape	D_n (mm)	E_n (mm)	F_n (mm)	R_n (mm)	N_n (mm)
13	First Sur. Window	5.000						Plane					4.0017
14	Second Sur. Window	0.380						Plane					1.0000
15	Detector Surface	2.063						Plane					1.0000

TABLE 4-14 (SHEET 1 OF 3). DIMENSIONAL PARAMETERS FOR CHANNEL 9 (TRANSMISSIVE)

Axis Sub-Script (n)	Optical Function of Surface	A_n (mm)	B_n (mm)	C_n (mm)	α_n (deg)	β_n (deg)	γ_n (deg)	Surface Shape	D_n (mm)	E_n (mm)	F_n (mm)	R_n (mm)	N_n (mm)
1	FOV Stop	98.440						Plane					1.0000
2	First Sur. Dichroic	9.000				-45.0		Plane					4.0017
3	Second Sur. Dichroic	1.000						Plane					1.0000
4	Mathematical Aid	-1.000				45.0		Plane					1.0000
5	First Sur. First Filter	10.000	-0.58					Plane					4.0017
6	Second Sur. First Filter	1.000						Plane					1.0000

TABLE 4-14 (SHEET 2 OF 3). DIMENSIONAL PARAMETERS FOR CHANNEL 9 (TRANSMISSIVE)

Axis Sub-Script (n)	Optical Function of Surface	A_n (mm)	B_n (mm)	C_n (mm)	α_n (deg)	β_n (deg)	γ_n (deg)	Surface Shape	D_n (mm)	E_n (mm)	F_n (mm)	R_n (mm)	N_n (mm)
7	First Sur. Second Filter	0.250						Plane					2.3740
8	Second Sur. Second Filter	1.750						Plane					1.0000
9	First Sur. First Lens	0.500						Sphere	1.0	1.0	1.0	17.456	4.0017
10	Second Sur. First Lens	1.550						Sphere	1.0	1.0	1.0	23.685	1.0000
11	First Sur. Second Lens	0.100						Sphere	1.0	1.0	1.0	10.128	4.0017

TABLE 4-14 (SHEET 3 OF 3). DIMENSIONAL PARAMETERS FOR CHANNEL 9 (TRANSMISSIVE)

Axis Sub-Script (n)	Optical Function of Surface	A_n (mm)	B_n (mm)	C_n (mm)	α_n (deg)	β_n (deg)	γ_n (deg)	Surface Shape	D_n (mm)	E_n (mm)	F_n (mm)	R_n (mm)	N_n (mm)
12	Second Sur. Second Lens	1.550						Sphere	1.0	1.0	1.0	11.567	1.0000
13	First Sur. Window	5.000						Plane					4.0017
14	Second Sur. Window	0.380						Plane					1.0000
15	Detector Surface	2.063						Plane					1.0000

TABLE 4-15 (SHEET 1 OF 3). DIMENSIONAL PARAMETERS FOR CHANNEL 10 (TRANSMISSIVE)

Axis Sub-Script (n)	Optical Function of Surface	A_n (mm)	B_n (mm)	C_n (mm)	α_n (deg)	β_n (deg)	γ_n (deg)	Surface Shape	D_n (mm)	E_n (mm)	F_n (mm)	R_n (mm)	N_n (mm)
1	FOV Stop	98.440						Plane					1.0000
2	First Sur. Dichroic	9.000				-45.0		Plane					4.0016
3	Second Sur. Dichroic	1.000						Plane					1.0000
4	Mathematical Aid	-1.000				45.0		Plane					1.0000
5	First Sur. First Filter	10.000	-0.58					Plane					4.0016
6	Second Sur. First Filter	1.000						Plane					1.0000

TABLE 4-15 (SHEET 2 OF 3). DIMENSIONAL PARAMETERS FOR CHANNEL 10 (TRANSMISSIVE)

Axis Sub-Script (n)	Optical Function of Surface	A_n (mm)	B_n (mm)	C_n (mm)	α_n (deg)	β_n (deg)	γ_n (deg)	Surface Shape	D_n (mm)	E_n (mm)	F_n (mm)	R_n (mm)	N_n (mm)
7	First Sur. Second Filter	0.250						Plane					2.3716
8	Second Sur. Second Filter	1.750						Plane					1.0000
9	First Sur. First Lens	0.500						Sphere	1.0	1.0	1.0	17.456	4.0016
10	Second Sur. First Lens	1.550						Sphere	1.0	1.0	1.0	23.685	1.0000
11	First Sur. Second Lens	0.100						Sphere	1.0	1.0	1.0	10.128	4.0016

TABLE 4-15 (SHEET 3 OF 3). DIMENSIONAL PARAMETERS FOR CHANNEL 10 (TRANSMISSIVE)

Axis Sub-Script (n)	Optical Function of Surface	A_n (mm)	B_n (mm)	C_n (mm)	α_n (deg)	β_n (deg)	γ_n (deg)	Surface Shape	D_n (mm)	E_n (mm)	F_n (mm)	R_n (mm)	N_n (mm)
12	Second Sur. Second Lens	1.550						Sphere	1.0	1.0	1.0	11.567	1.0000
13	First Sur. Window	5.000						Plane					4.0016
14	Second Sur. Window	0.380						Plane					1.0000
15	Detector Surface	2.064						Plane					1.0000

TABLE 4-16 (SHEET 1 OF 3). DIMENSIONAL PARAMETERS FOR CHANNEL 14 (TRANSMISSIVE)

Axis Sub-Script (n)	Optical Function of Surface	A_n (mm)	B_n (mm)	C_n (mm)	α_n (deg)	β_n (deg)	γ_n (deg)	Surface Shape	D_n (mm)	E_n (mm)	F_n (mm)	R_n (mm)	N_n (mm)
1	FOV Stop	98.440						Plane					1.0000
2	First Sur. Dichroic	9.000				-45.0		Plane					3.4100
3	Second Sur. Dichroic	1.000						Plane					1.0000
4	Mathematical Aid	-1.000				45.0		Plane					1.0000
5	First Sur. First Filter	10.000	-0.557					Plane					3.4100
6	Second Sur. First Filter	1.000						Plane					1.0000

TABLE 4-16 (SHEET 2 OF 3). DIMENSIONAL PARAMETERS FOR CHANNEL 14 (TRANSMISSIVE)

Axis Sub-Script (n)	Optical Function of Surface	A_n (mm)	B_n (mm)	C_n (mm)	α_n (deg)	β_n (deg)	γ_n (deg)	Surface Shape	D_n (mm)	E_n (mm)	F_n (mm)	R_n (mm)	N_n (mm)
7	First Sur. Second Filter	0.250						Plane					3.4100
8	Second Sur. Second Filter	1.000						Plane					1.0000
9	First Sur. First Lens	1.250						Sphere	1.0	1.0	1.0	15.677	3.4100
10	Second Sur. First Lens	1.550						Sphere	1.0	1.0	1.0	21.325	1.0000
11	First Sur. Second Lens	0.100						Sphere	1.0	1.0	1.0	8.912	3.4100

TABLE 4-16 (SHEET 3 OF 3). DIMENSIONAL PARAMETERS FOR CHANNEL 14 (TRANSMISSIVE)

Axis Sub-Script (n)	Optical Function of Surface	A_n (mm)	B_n (mm)	C_n (mm)	α_n (deg)	β_n (deg)	γ_n (deg)	Surface Shape	D_n (mm)	E_n (mm)	F_n (mm)	R_n (mm)	N_n (mm)
12	Second Sur. Second Lens	1.550						Sphere	1.0	1.0	1.0	10.500	1.0000
13	First Sur. Window	5.000						Plane					3.4100
14	Second Sur. Window	0.380						Plane					1.0000
15	Detector Surface	2.109						Plane					1.0000

TABLE 4-17. SUMMARY OF THE DESIGN AND PERFORMANCE OF THE SIXTEEN DETECTOR CHANNELS

Channel No.	λ (μ)	Telescope Diameter (mm)	Lens Radii, mm R_1 (mm)	R_2 (mm)	R_3 (mm)	R_4 (mm)	Beamsplitter Thickness/ Material Index-Refraction	Filter #1 Thickness/ Material Index-Refraction	Filter #2 Thickness Material Index-Refraction	Back Focal Distance* (mm)	Centroid Y (mm)	Maximum Radial Aberration ΔY (mm)	Estimated Half-Power Aberration 75% ΔY (mm)	Tangential Aberration ΔZ (mm)	Estimated Half-Power Aberration 75% ΔZ (mm)	(Ratio) 2Y / 75% ΔY
1	3.71	61	18.476	30.570	9.055	9.843		1.00 mm GE 4.0270	1.00 mm Sapphire 1.6875	6.394	0.7855	0.0153	0.0076	0.0294	0.0115	207:1
2	4.26	80	17.456	23.685	10.128	11.567		1.00 mm GE 4.0220	1.00 mm Sapphire 1.6637	7.383	0.9500	0.0196	0.0100	0.0197	0.0129	190:1
3	9.71	61	18.476	30.570	9.055	9.843		1.00 mm GE 4.0032	1.00 mm Irtran #2 2.2023	6.458	0.7936	0.0142	0.0073	0.0290	0.0119	217:1
4	11.13	61	18.476	30.570	9.055	9.843		1.00 mm GE 4.0026	1.00 mm Irtran #2 2.1825	6.459	0.7938	0.0142	0.0073	0.0290	0.0119	217:1
5	13.35	61	18.476	30.570	9.055	9.843	1.00 mm GE 4.0018	1.00 mm GE 4.0018	1.75 mm Irtran #4 2.3832	6.463	0.7958	0.0147	0.0073	0.0297	0.0108	218:1
6	13.61	61	18.476	30.570	9.055	9.843	1.00 mm GE 4.0018	1.00 mm GE 4.0018	1.75 mm Irtran #4 2.3815	6.463	0.7958	0.0147	0.0073	0.0297	0.0108	218:1
7	14.00	61	18.476	30.570	9.055	9.843	1.00 mm GE 4.0017	1.00 mm GE 4.0017	1.75 mm Irtran #4 2.3780	6.463	0.7959	0.0147	0.0073	0.0297	0.0108	218:1
8	14.30	80	17.456	23.685	10.128	11.567	1.00 mm GE 4.0017	1.00 mm GE 4.0017	1.75 mm Irtran #4 2.3756	7.443	0.9597	0.0198	0.0096	0.0193	0.0130	200:1
9	14.50	80	17.456	23.685	10.128	11.567	1.00 mm GE 4.0017	1.00 mm GE 4.0017	1.75 Irtran #4 2.3740	7.443	0.9597	0.0198	0.0096	0.0193	0.0130	200:1
10	14.84	80	17.456	23.685	10.128	11.567	1.00 mm GE 4.0016	1.00 mm GE 4.0016	1.75 mm Irtran #4 2.3716	7.444	0.9597	0.0198	0.0096	0.0193	0.0130	200:1
11	14.96	80	17.456	23.685	10.128	11.567		1.00 mm GE 4.0016	1.75 mm Irtran #4 2.3703	7.445	0.9622	0.0206	0.0098	0.0197	0.0134	197:1
12	18.80	80	15.677	21.325	8.912	10.500		1.00 mm Si 3.4140	1.75 mm Irtran #6 2.6470	7.477	0.9825	0.0099	0.0049	0.0402	0.0331	401:1
13	23.13	80	15.677	21.325	8.912	10.500		1.00 mm Si 3.4124	1.75 mm Irtran #6 2.6360	7.487	0.9832	0.0099	0.0047	0.0404	0.0322	419:1
14	29.40	80	15.677	21.325	8.912	10.500	1.00 mm Si 3.4100	1.00 mm Si 3.4100	1.00 mm Si 3.4100	7.489	0.9785	0.0094	0.0046	0.0392	0.0324	425:1

(1) Distance from second lens to image, including 0.38 mm cover plate.
All valves are negative in ray-trace.

The maximum radia spread for all 200 rays of a family of rays is given by ΔY and the maximum tangential spread for all 200 rays is given by ΔZ. The estimate half-power radial and tangential spreads are then 75 percent ΔY and 75 percent ΔZ, respectively. Finally, the last column of Table 4-17 shows how many times larger the centroid diameter of the detector is than its radial half-power aberrations. It is seen that the image on every detector has a half-power spread of less than 0.5 percent of the detector diameter. This means that the detector can be made only very slightly smaller than the image of the secondary mirror so as to receive maximum radiation from the telescope field-of-view without receiving the radiation which by-passes the telescope secondary mirror.

A second type of ray-trace shown in Figure 4-3 was performed to study the nature of the zonal illumination on the detector due to incoming radiation blockage by the secondary mirror. This is a ray trace of both reflective channel 11 and transmissive channel 8, which have respective dimensional parameters given by Tables 4-6 and 4-13. However, this ray trace commences with the (X_1, Y_1, Z_1) axis system, the field stop rather than the (X_o, Y_o, Z_o) axis system, the secondary mirror. The same 44 rays are used here for both channels 8 and 11, as were used for Figure 3-1, which includes the four main boundary rays of the 80-mm OD telescope. The three-directional cosines of 44 rays used for the Figure 3-1 ray trace are multiplied by (-1) so the rays are directed toward the detector optics. The image of these rays on the detector is seen to be very sharp at the detector periphery, but fuzzy at the boundaries of the central unilluminated area.

4.4 Error Analysis for the Detector Optical System

The purpose of this error analysis is to gain an understanding of the manufacturing and assembly tolerances which are necessary or desirable for each of the fourteen detector optical systems. Only the channel 5 optical system has been completely ray-traced for this error analysis, since it is typical of the dimensionally smaller detector optical systems, the performance characteristics of which are more affected by a given magnitude mechanical tolerance. Channel 5 is a transmissive channel, so to find the error effects of the reflective surface of the dichroic filter for a reflective channel,

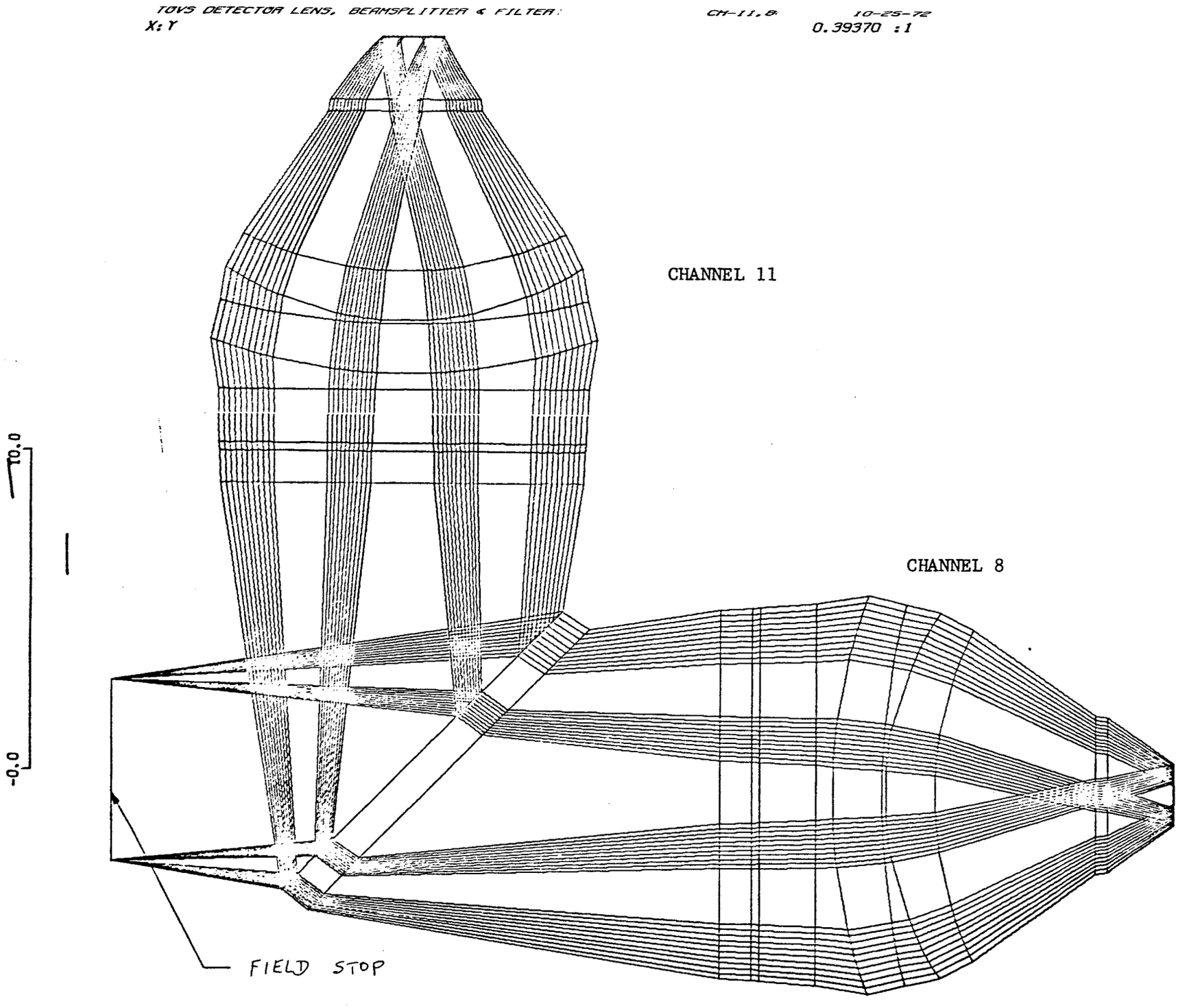

Figure 4-3. Zones of Illumination on the Detector Surface

channel 4 was used for this one analysis. Figure 4-2 shows the ray-trace axis systems and two boundary rays, which were used repeatedly for different error conditions within the detector optical systems. The axis systems of Figure 4-2 actually define, dimensionally, channels 8 and 11; however, transmissive channel 5 uses the same axis systems as channel 8, and reflective channel 4 uses the same axis system as channel 11.

The two rays marked E in Figure 4-2 start from a point on the lower edge of the telescope secondary mirror, intercept opposite edges of the field stop, and are imaged at the edge of the detector. These rays travel completely in the X-Y plane of each axis system for every error analysis, so the two-ray image is always at $Z_{15} = 0$ for channel 5, and $Z_{14} = 0$ for channel 4.

Table 4-18 describes the error performance of the channel 5 detector optical system for 54 different error conditions, besides its zero error condition, and Table 4-19 describes the error performance for the channel 4 detector optics for three error conditions. In order to gain an understanding of how each type of error can affect both the focus (longitudinal error) and the lateral image position (lateral error) of the secondary mirror image on the detector, only one type and magnitude of error is inserted into either channel 4 or 5 dimensional parameters at a time, and a ray trace is made with the same two starting rays E. For each ray trace, the computer automatically adjusts A_{15} for channel 5 and A_{14} for channel 4, the spacing between the detector window and the detector, until the two rays focus on the Y_{15}-Z_{15} and Y_{14}-Z_{14} planes, respectively. Table 4-18 gives the focused A_{15} and Y_{15} values for the zero error and the fifty four error conditions. Table 4-19 gives the focused A_{14} and Y_{14} values for the zero error and three error conditions. The columns following A and Y of these two tables show the change in that parameter relative to its zero error magnitude.

The nature of the errors described in Tables 4-18 and 4-19 are the spacing and thicknesses between the optical surfaces, A_3, A_{10}, A_{12}, and A_{14}; lateral shifts of lens or a lens surface, B_9, B_{10}, B_{11}, B_{12}, and B_{13}; changes in lens radii, R_9, R_{10}, R_{11}, and R_{12}; and changes in surface angles, β_2, β_4, β_6, and

TABLE 4-18 (SHEET 1 OF 3) ERROR ANALYSIS FOR CHANNEL 5 DETECTOR OPTICAL SYSTEM

Code	Description	A_{15}	(O) - (N) ΔA_{15}	Y_{15}	(O) - (N) ΔY_{15}
(0)	Zero Error	1.066231	0	0.803183	0
(1)	A_3 = 1.0025	1.066231	0	0.803152	0.000031
(2)	A_3 = 1.0250	1.066229	0.000002	0.802868	0.000315
(3)	A_3 = 1.2500	1.066177	0.000054	0.800033	0.003150
(4)	A_{10} = 1.5525	1.065267	0.000964	0.803146	0.000037
(5)	A_{10} = 1.5750	1.056600	0.009631	0.802814	0.000369
(6)	A_{10} = 1.8000	0.970040	0.096191	0.799473	0.003710
(7)	A_{12} = 1.5525	1.060835	0.005396	0.802717	0.000466
(8)	A_{12} = 1.5750	1.012486	0.053745	0.798531	0.004652
(9)	A_{12} = 1.8000	0.549096	0.517135	0.758145	0.045038
(10)	A_{14} = 0.3825	1.065696	0.000535	0.803194	-0.000011
(11)	A_{14} = 0.4050	1.060884	0.005347	0.803294	-0.000111
(12)	A_{14} = 0.6300	1.012761	0.053470	0.804290	-0.001107
(13)	B_9 = 0.0025, B_{10} = -0.0025	1.067086	-0.000855	0.806533	-0.003350
(14)	B_9 = 0.0250, B_{10} = -0.0250	1.074599	-0.008368	0.836712	-0.033529
(15)	B_9 = 0.2500, B_{10} = -0.2500	1.131424	-0.065193	1.141348	-0.338165
(16)	B_{10} = 0.0025, B_{11} = -0.0025	1.065814	0.000417	0.801285	0.001898
(17)	B_{10} = 0.0250, B_{11} = -0.0250	1.061997	0.004234	0.784213	0.018970
(18)	B_{10} = 0.2500, B_{11} = -0.2500	1.016873	0.049358	0.614734	0.188449
(19)	B_{11} = 0.0025, B_{12} = -0.0025	1.066355	-0.000124	0.809385	-0.006202
(20)	B_{11} = 0.0250, B_{12} = -0.0250	1.067034	-0.000803	0.865239	-0.062056
(21)	B_{11} = 0.2500, B_{12} = -0.2500	1.029204	0.037027	1.426134	-0.622851

TABLE 4-18 (SHEET 2 OF 3) ERROR ANALYSIS FOR CHANNEL 5 DETECTOR OPTICAL SYSTEM

Code	Description	A_{15}	O - N ΔA_{15}	Y_{15}	O - N ΔY_{15}
22	$B_{12} = 0.0025$, $B_{13} = -0.0025$	1.065661	0.000570	0.798285	0.004898
23	$B_{12} = 0.0250$, $B_{13} = -0.0250$	1.060039	0.006192	0.754255	0.048928
24	$B_{12} = 0.2500$, $B_{13} = -0.2500$	0.954757	0.111474	0.321479	0.481704
25	$R_9 = 18.4785$	1.067702	-0.001471	0.803356	-0.000173
26	$R_9 = 18.5010$	1.080938	-0.014707	0.804912	-0.001729
27	$R_9 = 18.7260$	1.212926	-0.146695	0.820409	-0.017226
28	$R_{10} = 30.5725$	1.065767	0.000464	0.803127	0.000056
29	$R_{10} = 30.5950$	1.061594	0.004637	0.802616	0.000567
30	$R_{10} = 30.8200$	1.020328	0.045903	0.797565	0.005618
31	$R_{11} = 9.0575$	1.071207	-0.004976	0.803798	-0.000615
32	$R_{11} = 9.0800$	1.116129	-0.049898	0.809345	-0.006262
33	$R_{11} = 9.3050$	1.579577	-0.513346	0.866523	-0.063340
34	$R_{12} = 9.8455$	1.063078	0.003153	0.802772	0.000411
35	$R_{12} = 9.8680$	1.034857	0.031374	0.799093	0.004090
36	$R_{12} = 10.0930$	0.766904	0.299327	0.764164	0.039019
37	$\beta_2 = -44.9975$, $\beta_4 = 44.9975$	1.066231	0.000003	0.803180	0.000003
38	$\beta_2 = -44.9750$, $\beta_4 = 44.9750$	1.066230	0.000013	0.803153	0.000030

TABLE 4-18 (SHEET 3 of 3). ERROR ANALYSIS FOR CHANNEL 5 DETECTOR OPTICAL SYSTEM

Code	Description	A_{15}	Ⓞ - Ⓝ ΔA_{15}	Y_{15}	Ⓞ - Ⓝ ΔY_{15}
39	β_2 = -44.7500, β_4 = 44.7500	1.066228	0.000003	0.802883	0.000300
40*	β_3 = -0.0025	1.066744	-0.000513	0.804765	-0.001582
41*	β_3 = -0.0250	1.071376	-0.005145	0.819012	-0.015829
42*	β_3 = -0.2500	1.118741	-0.052510	0.962498	-0.159315
43*	β_6 = -0.0025	1.066329	-0.000098	0.804221	-0.001038
44*	β_6 = -0.0250	1.067198	-0.000967	0.813563	-0.010380
45*	β_6 = -0.2500	1.074503	-0.008272	0.907097	-0.103914
46*	β_{14} = -0.0025	1.066424	-0.000193	0.803349	-0.000166
47*	β_{14} = -0.0250	1.068161	-0.001930	0.804844	-0.001661
48*	β_{14} = -0.2500	1.084993	-0.018762	0.819952	-0.016769
49	B_9 = 0.0025, B_{11} = -0.0025	1.066672	-0.000441	0.804634	-0.001451
50	B_9 = 0.0250, B_{11} = -0.0250	1.070616	-0.004385	0.817697	-0.914514
51	B_9 = 0.2500, B_{11} = -0.2500	1.107065	-0.040834	0.948798	-0.145615
52	B_{11} = 0.0025, B_{13} = -0.0025	1.065796	0.000435	0.804485	-0.001302
53	B_{11} = 0.0250, B_{13} = -0.0250	1.061910	0.004321	0.816196	-0.013013
54	B_{11} = 0.2500, B_{13} = -0.2500	1.025143	0.041088	0.932719	-0.129536

* Requires extra axis

TABLE 4-19. ERROR ANALYSIS FOR CHANNEL 4 DETECTOR OPTICAL SYSTEM

Code	Description	A_{14}	⓪ - Ⓝ ΔA_{14}	Y_{14}	⓪ - Ⓝ ΔY_{14}
⓪	Zero Error	1.062325	0	-0.800662	0
①	β_2 = -44.9975	1.062280	0.000045	-0.800063	-0.000599
②	β_2 = -44.9750	1.061878	0.000447	-0.794673	-0.005989
③	β_2 = -44.750	1.057886	0.004439	-0.740634	-0.060028

β_{14}. Each type of error was ray-traced for three different magnitudes, covering two deacdes, 0.0025 mm, 0.0250 mm, and 0.250 mm, which are equivalent, respectively, to 0.0001 inch, 0.0010 inch, and 0.0100 inch, or for 0.0025 degree, 0.0250 degree, and 0.2500 degree for the Beta angular errors.

Figure 4-4 is a plot of all the errors from Tables 4-18 and 4-19. Its log-log presentation of parameter error magnitude versus ΔA and ΔY shows that the errors are nearly linear over two decades. Thus, the different types of error values may be either added to or subtracted from each other. Figure 4-4 is next used to define the safe tolerance that may be placed on each parameter. Two horizontal lines are drawn, one at a ΔY value of 0.0161 mm, which is one percent of the diameter of the detector, and the other at the ΔA value of 0.0175 mm which represents a blur circle due to defocusing the f/1 detector image equal to one percent of the detector diameter. The intersection of the two decade error plots with these two horizontal lines, then, defines the respective parameter tolerances for one-percent ΔA and one-percent ΔY.

Table 4-20 shows the resultant errors in both millimeters and inches. Some of the errors are $>$0.2500 mm or $>$0.0100 inch, which means these errors have very little effect on the image. On the other hand, a lateral shift of B_9, B_{11}, and B_{12} of 0.0003 to 0.0004 inch is sufficient to produce a one-percent lateral field stop error.

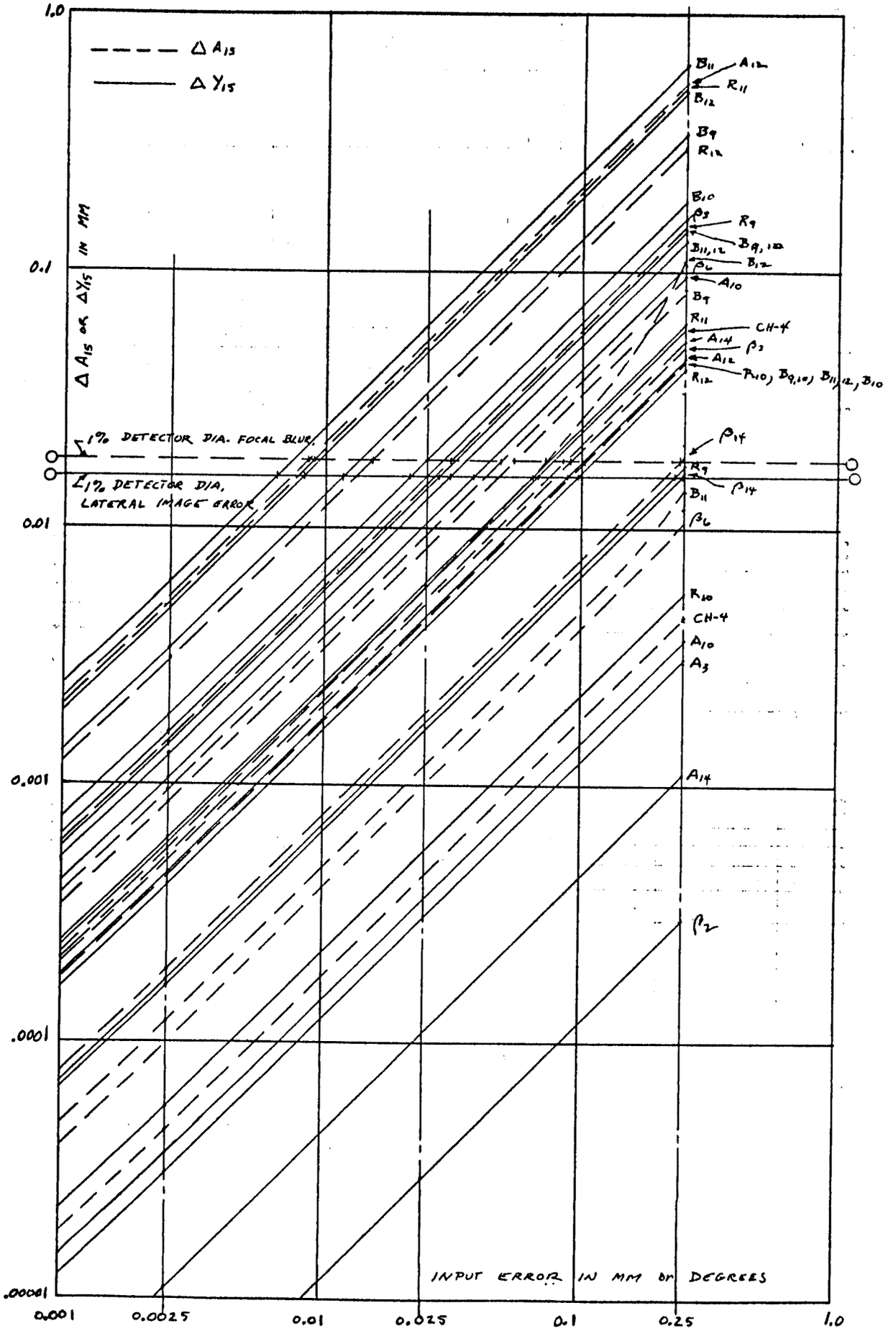

Figure 4-4. Channel 4 and 5 Error Analysis

TABLE 4-20. DIMENSIONAL TOLERANCES FOR ONE PERCENT DETECTOR IMAGE ERROR (CHANNELS 4 AND 5)

Description	Focal Error		Lateral Error	
	mm	Inches	mm	Inches
A_3	>0.2500	>0.0100	>0.2500	>0.0100
A_{10}	0.0460	0.0018	>0.2500	>0.0100
A_{12}	0.0082	0.0003	0.0880	0.0035
A_{14}	0.0820	0.0032	>0.2500	>0.0100
B_9	0.0550	0.0022	0.0120	0.0004
B_{10}	0.1050	0.0041	0.0210	0.0008
B_{11}	0.2400	0.0095	0.0066	0.0003
B_{12}	0.0640	0.0025	0.0084	0.0003
R_9	0.0300	0.0012	0.2350	0.0093
R_{10}	0.1000	0.0040	>0.2500	>0.0100
R_{11}	0.0089	0.0003	0.0640	0.0025
R_{12}	0.0140	0.0006	0.1020	0.0040
β_2 (Degrees) Tilt	>0.2500		>0.2500	
β_3 (Degrees) Wedge	0.0860		0.0255	
β_6 (Degrees) Wedge	>0.2500		0.0386	
β_{14} (Degrees) Wedge	0.2300		0.2450	
$B_{9,10}$	0.1050	0.0041	0.0280	0.0011
$B_{11,12}$	0.1050	0.0041	0.0300	0.0012
β_2 (CH-4) (Degrees) Tilt	>0.2500		0.0680	

5.0 DESIGN OF CHOPPER AND REFERENCE BLACKBODY

A reflective chopper is used to image the detector of each channel into a thermally-controlled and measured reference blackbody cavity. The light chopper chops the entering radiation just before it reaches the field stop. The chopper surface facing the field stop is a section of a concave toroid of circular cross-section, and has four equally spaced windows to give four chopping cycles per chopper rotation. During the chopping cycle, when the chopper blocks the field stop, the toroidal mirror images the detectors of both channels following it into a small blackbody cavity located on the chopper side of the field stop.

Separate toroidal mirror chopper surfaces have been designed by computer ray-tracing for the channels following the 61- and 80-mm telescopes, since these two-size telescopes are mounted on different radii. Figure 5-1 is a computer plot of the toroidal chopper mirror, used with the 61-mm OD telescope. It shows that the image of the detectors can be completely imaged within cavities having relatively small openings. Separate, but identical, cavities are used as the reference blackbody for each telescope.

Figure 5-1 shows three views of the ray-trace axis system. Tables 5-1 and 5-2 define the dimensional parameters for the toroidal choppers used with the 61- and 80-mm OD telescopes, respectively. Figure 5-2 is a spot diagram for the rays entering the reference cavity for the 61-mm telescope.

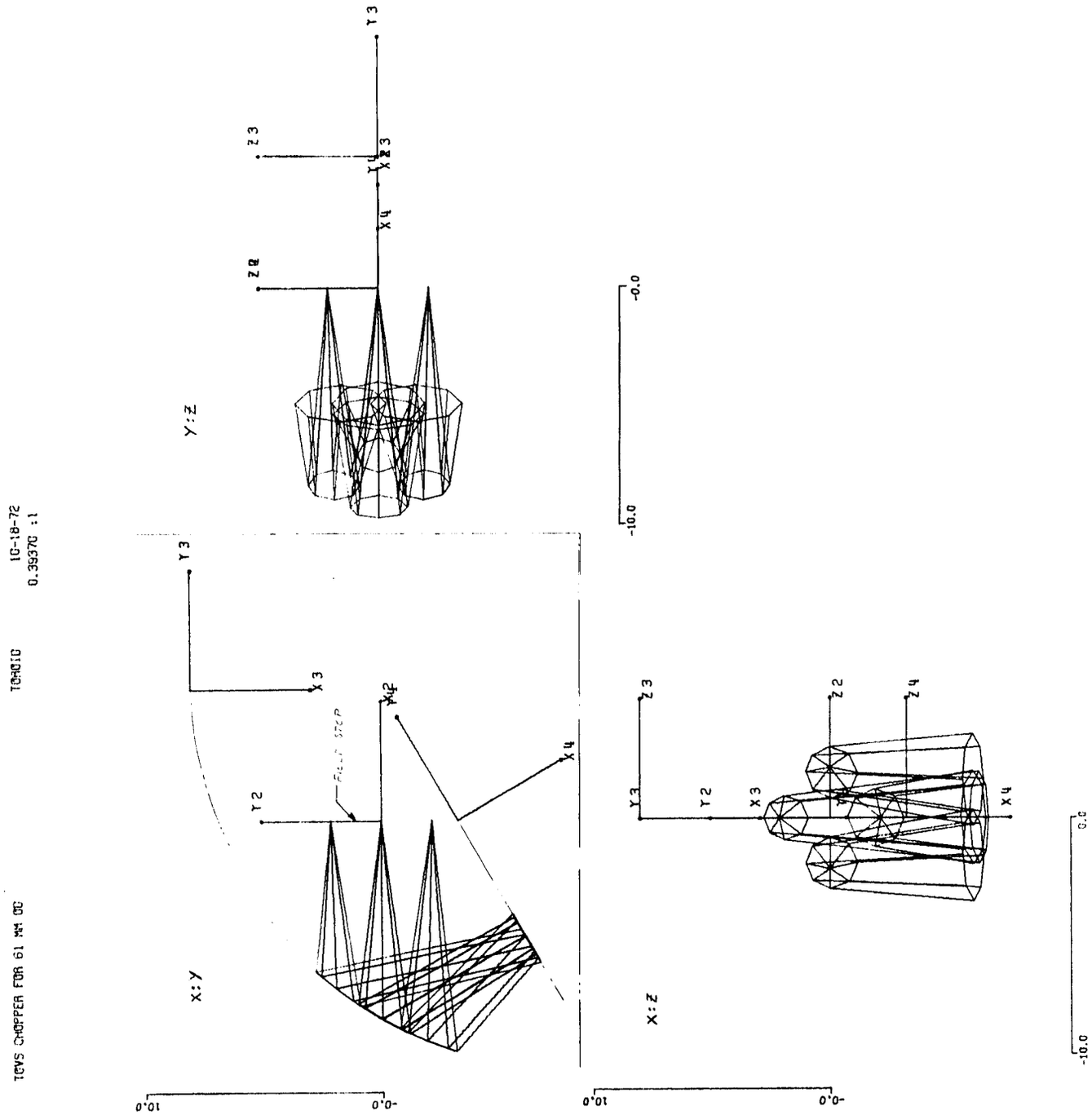

Figure 5-1. 3-View Ray-Trace Analysis of Toroidal Mirror for 61-MM OD Telescopes. The $(X_o,Y_o,Z_o,)$ and (X_1,Y_1,Z_1) axis systems are not plotted.

TABLE 5-1. DIMENSIONAL PARAMETERS FOR TOROIDAL CHOPPER FOR 61-MM OD TELESCOPE

Axis Sub-Script (n)	Optical Function of Surface	A_n (mm)	B_n (mm)	C_n (mm)	α_n (deg)	β_n (deg)	γ_n (deg)	Surface Shape	D_n (mm)	E_n (mm)	F_n (mm)	R_n (mm)	N_n (mm)
1	Secondary Mirror	-74.860						Sphere	1.0	1.0	1.0	-78.700	1.0000
2	Field Stop	74.860						Plane					1.0000
3	Toroid	5.580	8.043			-90.0		Toroid	Major Radius = 111.733				1.0000
									Minor Radius = 16.085				
4	Reference Cavity Opening	11.263	-5.580			45.0		Plane					1.0000

TABLE 5-2. DIMENSIONAL PARAMETERS FOR TOROIDAL CHOPPER FOR 80-MM OD TELESCOPE

Axis Sub-Script (n)	Optical Function of Surface	A_n (mm)	B_n (mm)	C_n (mm)	α_n (deg)	β_n (deg)	γ_n (deg)	Surface Shape	D_n (mm)	E_n (mm)	F_n (mm)	R_n (mm)	N_n (mm)
1	Secondary Mirror	-98.440						Sphere	1.0	1.0	1.0	-103.200	1.0000
2	Field Stop	98.440						Plane					1.0000
3	Toroid	8.975	14.951			-90.0		Toroid	Major radius = 108.303 Minor radius = 24.219				1.0000
4	Reference Cavity Opening	16.541	-8.975			45.0		Plane					1.0000

TOVS CHOPPER FOR 61 MM OD TOROID 10-18-72

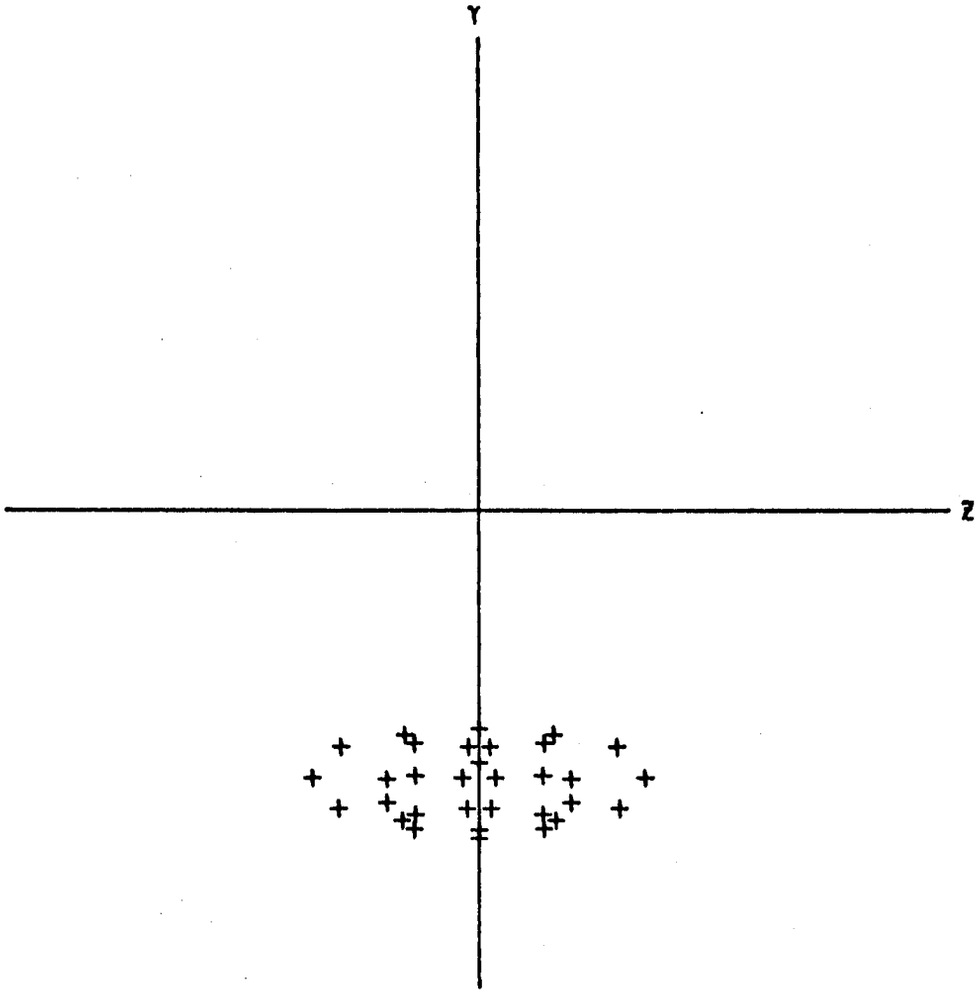

				MAX	MIN	
Z	HALF AXIS LENGTH	10.00000	Z =	3.5203	-3.5203	SURFACE NO.
Y	HALF AXIS LENGTH	10.00000	Y =	-4.7179	-6.5289	4

Figure 5-2. 32-Ray Spot Diagram Showing Detector Image Size at Reference Blackbody Opening for Toroid Chopper for 61-mm OD Telescope